Cell Reports

Article

Apolipoproteins L1 and L3 control mitochondrial membrane dynamics

Graphical abstract

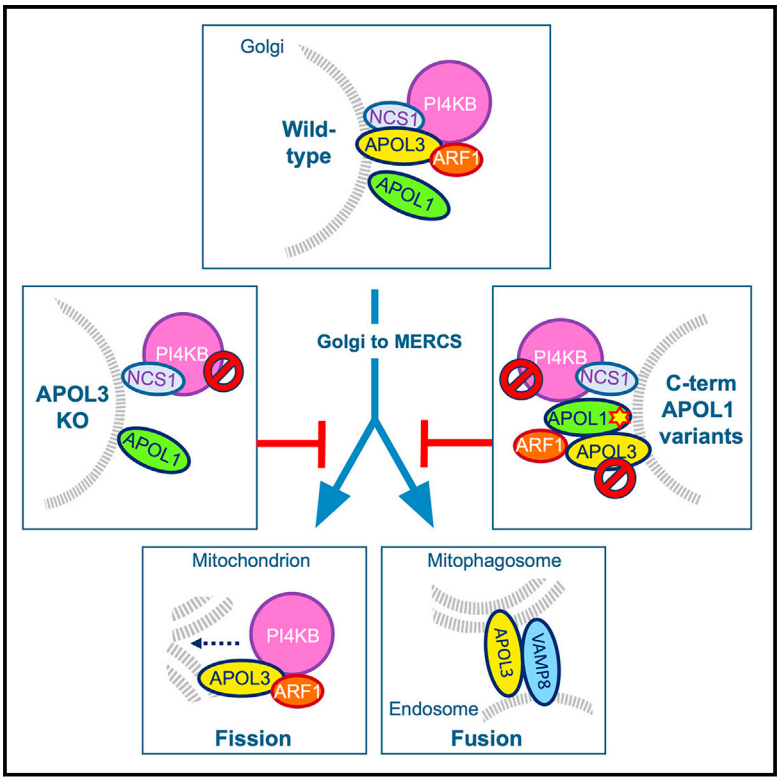

Highlights

- APOL3 controls the activity of the Golgi and mitochondrion membrane fission factor PI4KB
- APOL1 allows APOL3 and PI4KB traffic to MERCSs, linked to mitochondrion fission and mitophagy
- Through interaction with VAMP8, APOL3 promotes mitophagosome-endolysosome fusion
- C-terminal APOL1 variants reduce the mitophagy flux through APOL3 and PI4KB inactivation

Authors

Laurence Lecordier, Paul Heo, Jonas H. Graversen, ..., Frédéric Pincet, David Pérez-Morga, Etienne Pays

Correspondence

etienne.pays@gmail.com

In brief

Lecordier et al. report that APOL1 and APOL3 are involved in mitophagy. Whereas APOL1 mediates APOL3 and PI4KB traffic from the Golgi to MERCSs, APOL3 controls mitochondrial membrane fission and fusion through interactions with PI4KB and VAMP8, respectively. APOL1 C-terminal variants inhibit mitophagy through interference with APOL3 and PI4KB activities.

Lecordier et al., 2023, Cell Reports *42*, 113528
December 26, 2023
https://doi.org/10.1016/j.celrep.2023.113528

CellPress

Cell Reports

CellPress
OPEN ACCESS

Article

Apolipoproteins L1 and L3 control mitochondrial membrane dynamics

Laurence Lecordier,[1,6] Paul Heo,[2,3,6] Jonas H. Graversen,[4,6] Dorle Hennig,[4] Maria Kløjgaard Skytthe,[4] Alexandre Cornet d'Elzius,[1] Frédéric Pincet,[2] David Pérez-Morga,[1,5] and Etienne Pays[1,7,*]

[1]Laboratory of Molecular Parasitology, IBMM, Université Libre de Bruxelles, 6041 Gosselies, Belgium
[2]Laboratoire de Physique de l'Ecole Normale Supérieure, Ecole Normale Supérieure (ENS), Université Paris Sciences et Lettres (PSL), CNRS, Sorbonne Université, Université Paris-Cité, 75005 Paris, France
[3]Institute of Psychiatry and Neuroscience of Paris, INSERM U1266, 75014 Paris, France
[4]Department of Molecular Medicine, Cancer and Inflammation Research, University of Southern Denmark, 5000 Odense C, Denmark
[5]Center for Microscopy and Molecular Imaging (CMMI), Université Libre de Bruxelles, 6041 Gosselies, Belgium
[6]These authors contributed equally
[7]Lead contact
*Correspondence: etienne.pays@gmail.com
https://doi.org/10.1016/j.celrep.2023.113528

SUMMARY

Apolipoproteins L1 and L3 (APOLs) are associated at the Golgi with the membrane fission factors phosphatidylinositol 4-kinase-IIIB (PI4KB) and non-muscular myosin 2A. Either APOL1 C-terminal truncation (APOL1Δ) or APOL3 deletion (APOL3-KO [knockout]) reduces PI4KB activity and triggers actomyosin reorganization. We report that APOL3, but not APOL1, controls PI4KB activity through interaction with PI4KB and neuronal calcium sensor-1 or calneuron-1. Both APOLs are present in Golgi-derived autophagy-related protein 9A vesicles, which are involved in PI4KB trafficking. Like APOL3-KO, APOL1Δ induces PI4KB dissociation from APOL3, linked to reduction of mitophagy flux and production of mitochondrial reactive oxygen species. APOL1 and APOL3, respectively, can interact with the mitophagy receptor prohibitin-2 and the mitophagosome membrane fusion factor vesicle-associated membrane protein-8 (VAMP8). While APOL1 conditions PI4KB and APOL3 involvement in mitochondrion fission and mitophagy, APOL3-VAMP8 interaction promotes fusion between mitophagosomal and endolysosomal membranes. We propose that APOL3 controls mitochondrial membrane dynamics through interactions with the fission factor PI4KB and the fusion factor VAMP8.

INTRODUCTION

The function of human apolipoprotein L1 and L3 (APOLs) is largely unknown, except that secreted APOL1 exhibits efficient trypanosome-killing activity, which confers protection against infection by the African bloodstream parasite *Trypanosoma brucei*.[1,2] Owing to their distinct mechanisms of resistance to APOL1, the *T. brucei* subspecies *T. b. rhodesiense* in Eastern Africa and *T. b. gambiense* in Western Africa can infect humans and cause sleeping sickness.[3] In Western Africa, many people express C-terminal APOL1 variants termed G1 and G2, which circumvent *T. b. rhodesiense* resistance and thus can kill this parasite.[4] However, expression of G1 or G2 is linked to increased susceptibility to chronic kidney disease, especially during interferon (IFN)-I-mediated inflammation, as occurs upon viral infection.[4–8] The effects of APOL1 variants on kidney podocytes are called hit 1 and hit 2 in the absence and presence of viral infection, respectively. How G1 and G2 trigger kidney disease has been debated for years but remains uncertain.[6,7,9–12]

APOL1 and APOL3 can form membrane pores, but transmembrane insertion of APOL1 requires an acidic pH.[13,14] These proteins are present in minute amounts at Golgi and endoplasmic reticulum (ER) membranes, in close contact with phosphatidylinositol-4-kinase-IIIB (PI4KB), neuronal calcium sensor-1 (NCS1), and non-muscular myosin 2A (NM2A).[11] APOL3 specifically interacts with the PI4KB activator NCS1 and can stimulate PI(4)P synthesis *in vitro*. Accordingly, deletion of the APOL3 gene (APOL3-KO [knockout]), but not that of the APOL1 gene, was linked to reduced Golgi PI4KB activity, associated with important Golgi shrinkage and actomyosin reorganization, characteristics also observed in natural G1/G2 podocytes.[11] Consistently, kidney disease was also linked to natural loss of APOL3,[15] and the G1/G2 variants were found to inactivate APOL3 through increased interaction.[11] Such interaction with APOL3 resulted from G1/G2 mutations in the C-terminal leucine zipper helix LZ2 that disrupt LZ2 *cis*-interaction with an N-terminal LZ (LZ1) and lead to increased APOL1 hydrophobicity.[11] As occurs for the G1 or G2 variants, deletion of LZ2 (in APOL1Δ) triggered APOL1 unfolding and increased APOL1 interaction with APOL3, inducing a G1/G2-like phenotype linked to reduction of PI4KB activity, albeit with higher severity.[11] Thus, either APOL3 absence or APOL3 inactivation by APOL1 LZ2 variants (G1, G2, or APOL1Δ) can affect PI4KB activity, causing podocyte dysfunctions resembling those associated with kidney disease.

PI4KB is involved with NM2A in membrane fission for secretion at the *trans*-Golgi or for mitochondrial division.[16–20] Consequently,

interference with PI4KB due to APOL3 absence or inactivation could affect Golgi and/or mitochondrial membrane fission. However, PI4KB and APOL3 are also present within the nucleus,[11,21,22] where PI4KB and PI(4)P are associated with mRNA speckles and factors involved in pre-mRNA splicing and nuclear transport.[23,24] Thus, interference with APOL3-PI4KB interaction may also alter gene expression. Accordingly, NCS1 deficiency affects mRNA levels of genes involved in mitochondrial activity.[25]

Besides indirect effects through PI4KB control, APOL1 and APOL3 may also directly act on mitochondrial membranes. Both APOL1 and APOL3 bind to the mitochondrion-specific phospholipid cardiolipin,[11] and APOL1 strongly associates with mitochondrial membranes following *in vitro* incubation[26] or ectopic expression in yeast.[27] Specifically, APOL1 or APOL3 may affect mitochondrial membrane fusion, which involves cardiolipin.[28] Indeed, APOL1 or APOL3 uptake in trypanosomes is linked to increased mitochondrial fusion,[14,26] and APOL3 exhibits fusion activity on cardiolipin-rich bacterial membranes.[29]

Podocyte dysfunctions associated with viral infection (hit 2) are linked to strongly increased expression of APOL1 or APOL1 variants by inflammatory IFN-I signaling, triggered by either IFN-β or the viral mimetic poly(I:C).[11,30,31] Viral infections induce auto-/mitophagy.[32–37] Autophagy depends on NM2A-driven trafficking of PI4KB-containing vesicles from the Golgi to the pre-autophagosomal structure or phagophore-assembly site (PAS).[38–41] Different viruses benefit from this process, hijacking PI4KB to build their replication platforms.[42–45] Interestingly, this proviral activity involves APOL3.[46] G1/G2 hit 2 could result from interference with virus-induced autophagy, as reducing autophagy particularly affects podocytes,[47] and autophagy is crucial to digest viral aggresomes.[48] Because G1/G2 expression causes dysfunction of both autophagy and mitochondrion activity,[49–51] the APOL1 variants may specifically perturb mitophagy, induced at mitochondrion-ER contact sites (MERCSs) to maintain mitochondrial function despite membrane damage due to the inflammatory reaction.[33,52–56]

Here, we discovered that APOL1 and APOL3 control mitochondrial membrane dynamics and thus mitophagy. Interaction with the membrane fission factor PI4KB, along with structural and functional similarities to the membrane fusion factors soluble-N-ethylmaleimide-sensitive factor attachment receptor (SNARE) proteins, explains the involvement of APOL3 in dual membrane fission and fusion activities.

RESULTS

APOL3, but not APOL1, binds to PI4KB and controls PI4KB activity

Using biolayer interferometry (BLI), we previously demonstrated the Ca^{2+}-dependent interaction of APOL3, but not APOL1, with the PI4KB activator NCS1.[11] Substrate-immobilized NCS1 did not interact with PI4KB unless PI4KB was previously bound to APOL3, thus forming a trimeric complex. Here, we used immobilized PI4KB to analyze its interaction with NCS1 and APOL3. PI4KB exhibited a Ca^{2+}-independent interaction with both APOL3 and NCS1, separately or in succession (Figures 1A–1C). Thus, the lack of NCS1 interaction with PI4KB in our previous study likely resulted from NCS1 immobilization that involves unspecific lysine biotinylation. The binding affinities (K_d) of PI4KB for APOL3 and NCS1 were 11.7 and 34.7 nM, respectively (Figure S1A). In contrast to APOL3, APOL1 only weakly interacted with PI4KB (Figure 1A).

NCS1 and calneuron-1 (CALN1) are calmodulin-like proteins that inversely control Golgi PI4KB activity dependent on Ca^{2+} concentration.[57] Unlike NCS1, CALN1 interacted with APOL3 in the absence of Ca^{2+} (Figure 1D). The K_d for the CALN1-APOL3 interaction was 13.8 nM (Figure S1A). Like NCS1, CALN1 did not interact with APOL1 (Figure 1D).

APOL3 can stimulate *in vitro* PI4KB activity in the presence of Ca^{2+}.[11] As expected from its inhibitory function dependent on Ca^{2+} absence,[57] CALN1 reduced PI4KB activity under these conditions (Figure 1E). When Ca^{2+} was present, APOL3 reversed the CALN1-mediated inhibition of PI4KB (Figure 1E).

We conclude that APOL3 interacts with PI4KB and with either NCS1 or CALN1 depending on Ca^{2+}. Because NCS1 is not required for Ca^{2+}-dependent PI4KB stimulation by APOL3 *in vitro*, we propose that the *in vivo* role of NCS1 is to provide Ca^{2+} locally for Golgi PI4KB activation by APOL3.

APOL3 and NCS1 bind to three helices in the regulatory N-terminal domain of PI4KB

To determine the NCS1- and APOL3-binding sites in PI4KB, we compared PI4KB and NCS1 with their yeast homologs phosphatidylinositol-4-kinase-1 (PIK1) and frequenin-1 (FRQ1). In PIK1, FRQ1 binds between the binding sites of Ras-related protein-11 (RAB11) and ADP-ribosylation-factor binding protein-2A (GG2A), which are also present in PI4KB (Figure S1B). Because FRQ1 interacts with GGA2 for PIK1 function,[58] and because NCS1 can efficiently replace FRQ1 in yeast,[59] we hypothesized that NCS1 can bind near the GGA2-binding region of PI4KB.

In the N-terminal domain of PI4KB, the region between the RAB11A- and GGA2-binding sites differs greatly from the corresponding sequence in PIK1 and is organized in a three-helix bundle (H1-H3) (Figure S1C). Surface plasmon resonance (SPR) showed interaction of synthetic PI4KB H1-H3 peptides with both APOL3 and NCS1 and at lower levels with APOL1 or with a NCS1 mutant (L89K) exhibiting reduced interaction with APOL3[11] (Figures 2A, S1D, and S1E). Mutating or deleting individual PI4KB helices, particularly H1 and H3, severely reduced APOL3 and NCS1 binding (Figure S1E).

Thus, in addition to their Ca^{2+}-dependent interaction, APOL3 and NCS1 directly interact with a three-helix bundle in the N-terminal regulatory domain of PI4KB (H1-H3), forming a trimeric complex.

NCS1 binds to APOL3 hydrophobic cluster 1 (HC1)

NCS1 is known to interact with hydrophobic peptides,[60] and the H1 and H3 peptides of PI4KB are hydrophobic. Accordingly, the APOL3 site of interaction with NCS1 was proposed to be a C-terminal HC (HC2), given the decreased NCS1 binding to APOL3 following reduction of HC2 hydrophobicity.[11] In APOL1, HC2 and an N-terminal HC (HC1) form with respective downstream leucine zippers (C-terminal LZ2 and N-terminal LZ1) two HC-LZ tandems that interact in *cis*, the smallest interacting domains being K78-Q121 and V346-K390.[11] This *cis*-interaction, predicted to form a four-helix bundle (Figure S2A), is prevented at low pH

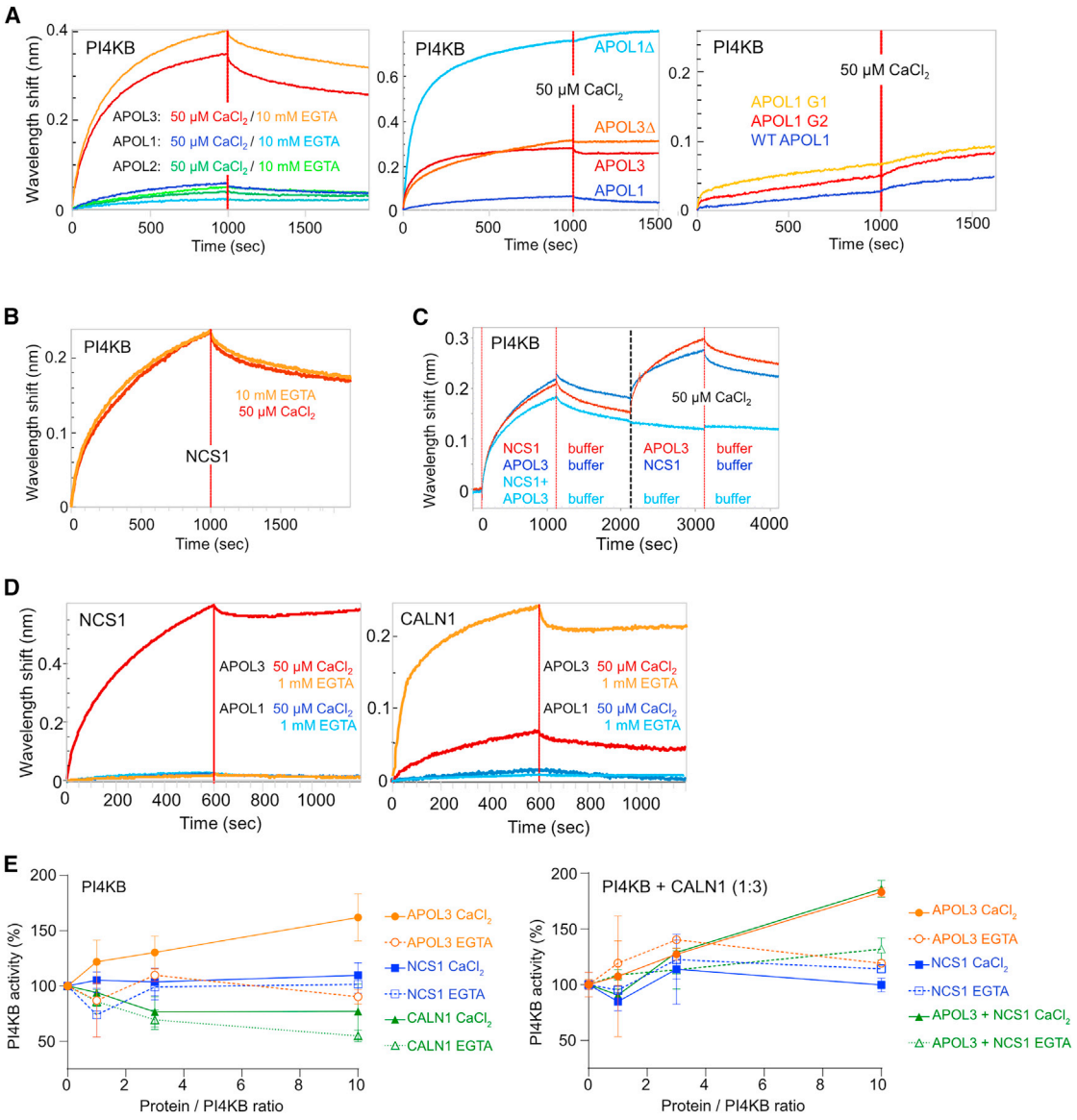

Figure 1. Interactions between PI4KB, APOLs, NCS1, and CALN1

(A) BLI measurements of immobilized PI4KB interaction with various recombinant APOLs, with or without calcium as indicated (n = 3).

(B) BLI measurements of immobilized PI4KB interaction with recombinant NCS1 with or without calcium (n = 3).

(C) BLI measurements of immobilized PI4KB sequential interaction with recombinant APOL3 and NCS1 as indicated (n = 3).

(D) BLI measurements of immobilized NCS1 (left) or CALN1 (right) interaction with recombinant APOL1 or APOL3 with or without calcium (n = 3).

(E) PI(4)P synthesis by recombinant PI4KB (50 ng) with or without addition of different recombinant proteins, expressed as percentage of activity without addition. The activity without PI substrate or without PI4KB (<0.1%) was subtracted (n = 3). PI4KB was mixed with a 3-fold stoichiometric amount of CALN1 as shown on the right. Error bars represent the standard deviation.

(Figure 2B). Such interaction was not observed in APOL3,[11] likely owing to lower interaction potential between the N- and C-terminal domains (Figure S2A).

We evaluated the binding of NCS1 to synthetic HC peptides from either APOL3 or APOL1 (Figure S1F). NCS1 interacted with APOL3 HC1 rather than with APOL3 HC2 as proposed previously. Conversely, NCS1 only interacted weakly with APOL1 HC1. Thus, NCS1 primarily interacts with HC1, in APOL3 only. Since NCS1 or FRQ1 can simultaneously bind two distinct hydrophobic peptides,[60,61] HC2 could strengthen the HC1-NCS1 interaction (scheme in Figure S1G).

Contrasting with APOL1, C-terminally truncated APOL1 (APOL1Δ) binds to PI4KB

C-terminal truncation of APOL1, which removes LZ2 (in APOL1Δ), disrupts *cis*-interaction with LZ1, allowing surface exposure of HCs and increased interaction with APOL3, leading to a G1/G2-like phenotype with increased severity.[11] Accordingly, APOL1Δ

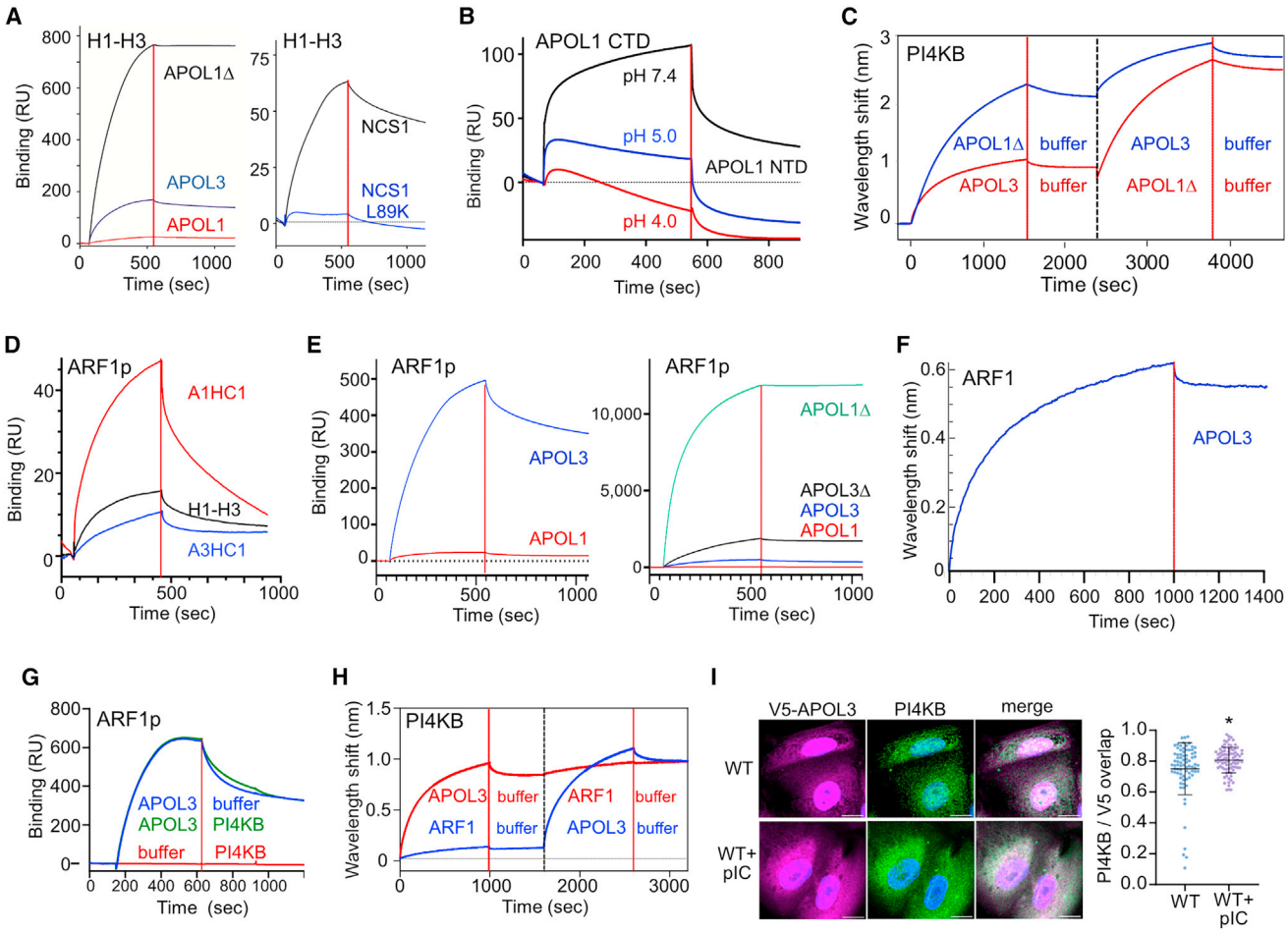

Figure 2. *Cis*- and *trans*-interactions of APOL1, APOL3, PI4KB, and ARF1

(A) Representative SPR sensorgrams of immobilized PI4KB H1-H3 interactions with recombinant APOL1, APOL1Δ, APOL3, NCS1, or NCS1 L89K (n = 3). As in (B)–(I), interaction was performed in 50 μM $CaCl_2$.

(B) SPR sensorgrams of immobilized APOL1 CTD interaction with the APOL1 NTD peptide, measured at different pHs (n = 3).

(C) BLI measurements of immobilized PI4KB sequential interactions with recombinant APOL1Δ or APOL3 as indicated (n = 3).

(D) Representative SPR sensorgrams of immobilized ARF1p interaction with PI4KB H1-H3 or APOL1/3 HC1 peptides (n = 3).

(E) Representative SPR sensorgrams of immobilized ARF1p interaction with recombinant APOL3, APOL1, APOL3Δ, or APOL1Δ (n = 3). Notice the different binding scales between the two graphs.

(F) BLI measurement of immobilized recombinant ARF1 interaction with recombinant APOL3 (n = 3).

(G) Representative SPR sensorgrams of immobilized ARF1p sequential interactions with recombinant APOL3 or PI4KB as indicated (n = 3).

(H) BLI measurements of immobilized PI4KB sequential interactions with recombinant APOL3 or ARF1 as indicated (n = 3).

(I) Immunofluorescence analysis of APOL3-V5 co-localization with PI4KB in WT podocytes treated or not with poly(I:C). Bar: 20 μm; blue: nucleus (DAPI). n = 3; Mann-Whitney test, *p < 0.05. Error bars represent the standard deviation.

and APOL1 HC peptides interacted strongly with APOL3 HC1 (Figure S1F). Unexpectedly, this truncation was necessary and sufficient to also confer high-affinity binding of APOL1Δ to PI4KB (K_d = 31.8 nM), whereas a similar truncation in APOL3 did not affect PI4KB binding (Figure 1A). Moreover, APOL1Δ interacted much better than did APOL1 with the PI4KB H1-H3 peptide (Figure S1E). This interaction was also stronger than that of APOL3 (Figure 2A) and more specifically involved the PI4KB H1 helix (Figure S1E). The strong APOL1Δ interaction with PI4KB may result from a higher degree of coiled coiling of APOL1 HC1 over that of APOL3 HC1 (Figure S1H). Sequential interactions of APOL1Δ and APOL3 with PI4KB led to cumulative binding (Figure 2C), in accordance with the APOL1Δ potential to interact with both APOL3 and PI4KB.

Contrasting with APOL1Δ, the G1 and G2 variants only weakly interacted with PI4KB (Figure 1A). Thus, *cis*-interaction between the two HC-LZ tandems appeared to prevent APOL1 binding to PI4KB, and LZ2 deletion relieved this inhibition more strongly than LZ2 G1/G2 mutations.

APOL3 interacts with ADP-ribosylation factor-1 (ARF1)

For PI4KB recruitment to the Golgi membrane, activated ARF1 (GTP bound) interacts with PI4KB and NCS1,[62–64] and in yeast, activated ARF1 paralogs bind to the PIK1-FRQ1 complex.[65]

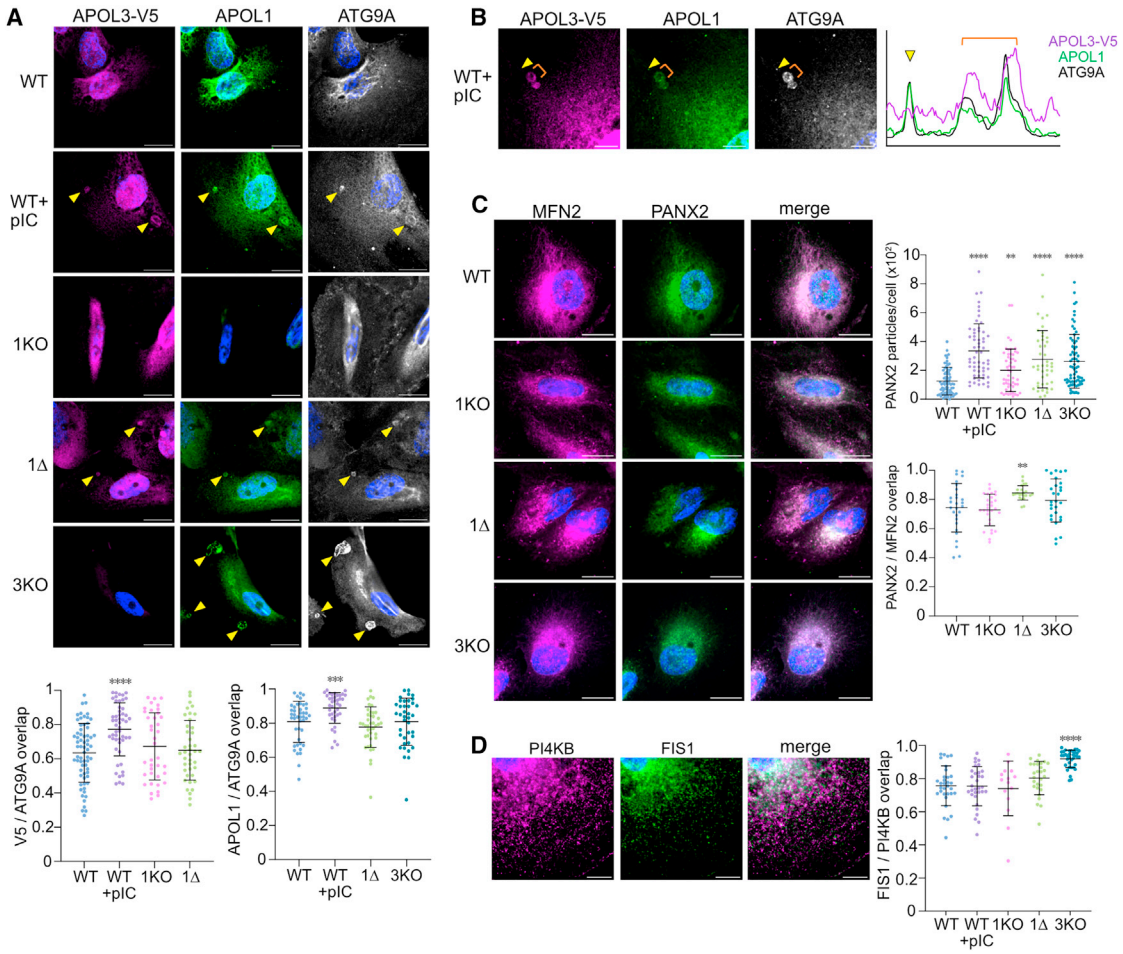

Figure 3. Cellular changes linked to APOL1/-3 gene editing

(A) Immunofluorescence analysis of APOL3-V5 and APOL1 co-localization with ATG9A vesicles in various podocyte cell lines. The arrowheads point to coalesced vesicles. Bar: 20 μm; blue: nucleus (DAPI). n = 3; Mann-Whitney test, ***p < 0.001; ****p < 0.0001. Error bars represent the standard deviation.

(B) Co-localization of APOL3-V5 and APOL1 with ATG9A in coalesced ATG9A vesicles of WT podocytes incubated with poly(I:C). Arrowhead: co-localization of ATG9A with APOL1 occurring only in non-coalesced vesicle. Bar: 10 μm.

(C) Immunodetection of the MERCS marker PANX2 in different podocyte cell lines and co-localization of PANX2 with MFN2. Bar: 20 μm; blue: nucleus (DAPI). n = 3; Mann-Whitney test, **p < 0.01; ****p < 0.0001. Error bars represent the standard deviation.

(D) Co-localization of PI4KB with FIS1 in various podocyte cell lines. Bar: 10 μm; blue: nucleus (DAPI). n = 3; Mann-Whitney test, ****p < 0.0001. Error bars represent the standard deviation.

The S93-H145 region of ARF1, which includes the α3 and α4 helices,[66] structurally resembles HC1-LZ1 of APOL3 (corresponding to APOL1 helices 2–4 in Ultsch et al.[67]) and both PI4KB H1-H3 and the FRQ1-binding region of PIK1 (Figure S3). Consistently, the synthetic ARF1 S93-H145 peptide (ARF1p) interacted at a similar level with PI4KB H1-H3 and APOL3 HC1 (Figure 2D). This interaction was greater with APOL1 HC1, likely owing to its higher coiling potential (Figure S1H). ARF1p showed high binding to APOL3 and APOL3Δ and very high binding to APOL1Δ, but not to APOL1 (Figure 2E). Accordingly, recombinant ARF1 interacted with APOL3 (Figure 2F). Independently of APOL3 binding, ARF1p did not interact with PI4KB (Figure 2G), and recombinant ARF1 only weakly interacted with PI4KB (Figure 2H). *In vivo*, this interaction requires ARF1 activation and association with NCS1.[62–64]

As ARF1 can bind APOL3, it may affect APOL3-NCS1-PI4KB interaction. However, PI4KB remained associated with APOL3 in cells treated with poly(I:C), where ARF1 is activated (Figure 2I).

APOL3 and APOL1 are present in ATG9A vesicles

Given the binding of APOL3 to PI4KB, we analyzed the possible association of APOL3 and APOL1 with autophagy-related protein 9A (ATG9A) vesicles, known to traffic PI4KB from the Golgi.[40,41] Immunofluorescence revealed co-localization of both APOLs with ATG9A, APOL1 being more frequently associated with ATG9A than APOL3 (Figure 3A). Poly(I:C) clearly increased the association of both APOLs with ATG9A (Figure 3A). Because PI4KB is involved in autophagy[40] and

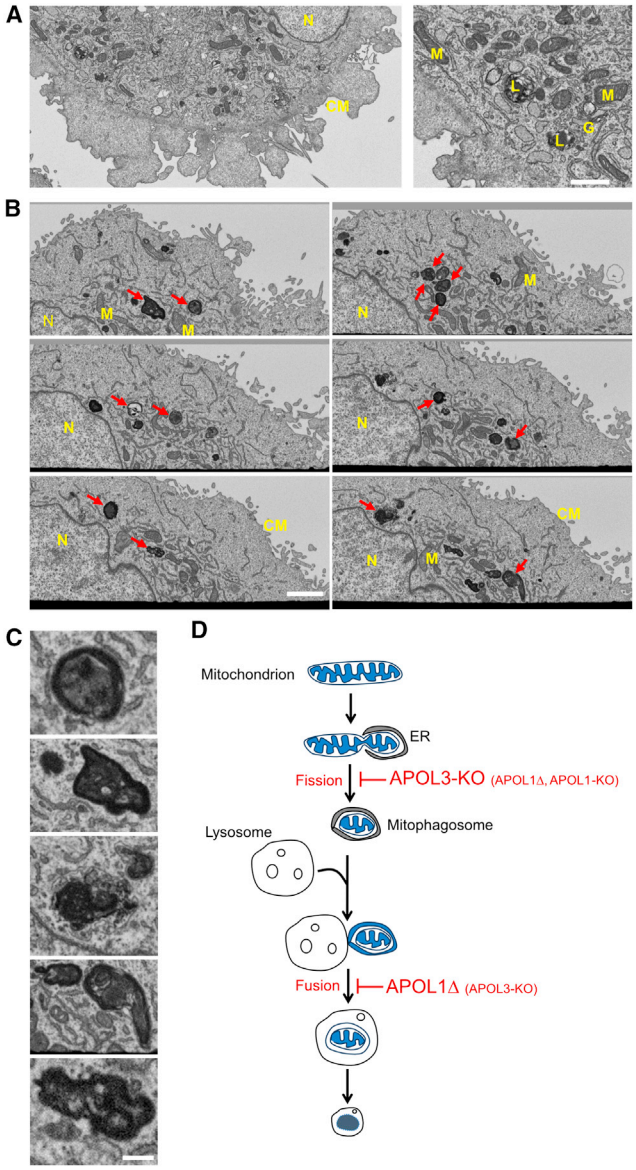

Figure 4. Mitochondrial structures in WT and APOL1Δ podocytes

(A) Representative images of the cytoplasm of WT podocytes in independent sections of the same cell volume imaged by FIB-SEM. N, nucleus, CM, cytoplasmic membrane; L, lysosome; G, Golgi; M, normal mitochondrion. Bars: 1 μm.

(B) Same as (A) but in APOL1Δ podocytes. Arrows point to mitophagosomes at several stages of maturation. Notice the decrease in cytoplasmic membrane complexity due to actomyosin cytoskeleton changes.[11] Bars: 2 μm.

(C) Zoom in on some of the mitophagosomes in (B). Bars: 250 nm.

(D) Model of mitophagosome formation in the different podocyte cell lines. In APOL1Δ cells, the delay in mitophagosome resolution leads to its increase in size and complexity, with the emergence of multilamellar bodies attached to the mitochondrion.

ATG9A is a lipid scramblase driving expansion of the PAS membrane early in autophagy,[68–71] the association of APOL1 and APOL3 with PI4KB and ATG9A suggests an autophagy-related function.

Like viral signaling, interference with APOL3 activity induces ATG9A vesicle coalescence and MERCS formation

IFN-I signaling induced by viral infection or by the viral mimetic poly(I:C) triggers PI4KB delocalization, mitochondrion fission, and auto-/mitophagy.[33,44,45,72–74] Consistently, poly(I:C) induced APOL3 dissociation from the Golgi[11] and led to APOL3 association with APOL1 in coalesced ATG9A vesicles (Figure 3B). Poly(I:C) also increased the number of particles bearing the MERCS marker pannexin-2 (PANX2)[75] (Figure 3C), which co-localizes with mitofusin-2 (MFN2), another MERCS marker[76] (Figure 3C).

Without induction of IFN-I signaling, APOL3-KO and APOL1Δ cells contained both coalesced ATG9A vesicles (Figure 3A) and increased numbers of PANX2 particles (Figure 3C). Thus, as with poly(I:C), APOL3 deletion or APOL1Δ expression appeared to trigger ATG9A vesicle coalescence and MERCS formation. Moreover, slightly in APOL1Δ cells and strongly in APOL3-KO cells, co-localization of PI4KB with the mitochondrial fission-1 protein (FIS1) was increased (Figure 3D). Since FIS1 is present in MERCSs,[77,78] this observation suggested that interference with APOL3 activity increases PI4KB transfer to MERCSs.

Interference with APOL3 activity reduces mitophagy

Using *in vivo* incorporation of the fluorescent CMXRos MitoTracker that accumulates in mitochondria and some mitophagosomes,[79] we showed previously that APOL1Δ and APOL3-KO cells, but not APOL1-KO cells, contain more small globular mitochondria than wild-type (WT) podocytes.[11] To explore this phenotype further, we used tomography by focused ion beam-scanning electron microscopy (FIB-SEM). This revealed reduced mitophagy rates in APOL1Δ and APOL3-KO podocytes (Figures 4A–4D and 5A–5D), with accumulation of both mitochondrial membrane-budding structures indicating unresolved fission (Figures 5D, S4C, S4D, and S5) and mitochondrion-derived dark, convoluted, and multilamellar mitophagosomes indicating unresolved mitophagosome-endolysosome fusion (Figures S4C, S4D, and S5). The unresolved fission and fusion structures were predominant in APOL3-KO and APOL1Δ cells, respectively (Figures 5B and 5D). In APOL1-KO cells, the number of mitophagosomes was strongly reduced, likely owing to accumulation of unresolved fission structures (Figures 5B–5D).

Thus, the mitophagy flux was decreased in both APOL3-KO and APOL1Δ cells, and mitophagy was inhibited in APOL1-KO cells (scheme in Figure 4D).

Interference with APOL3 activity induces mitochondrial reactive oxygen species (ROS) production

ROS generation is associated with mitochondrial dysfunction.[80] This phenomenon occurred in both APOL3-KO and APOL1Δ cells and at a lower level in APOL1-KO cells (Figure 5E). These conditions mimic IFN-I-mediated signaling because incubating WT cells with poly(I:C) also resulted in mitochondrial ROS generation (Figure 5E).

Thus, APOL3 absence or inactivation affects mitochondrial activity as occurs under inflammatory conditions.

APOL1 can bind to the mitophagy receptor PHB2

Mouse APOL9, which, like APOL1 and APOL3, is strongly induced by IFN-β, binds to prohibitin-2 (PHB2) in virus-infected

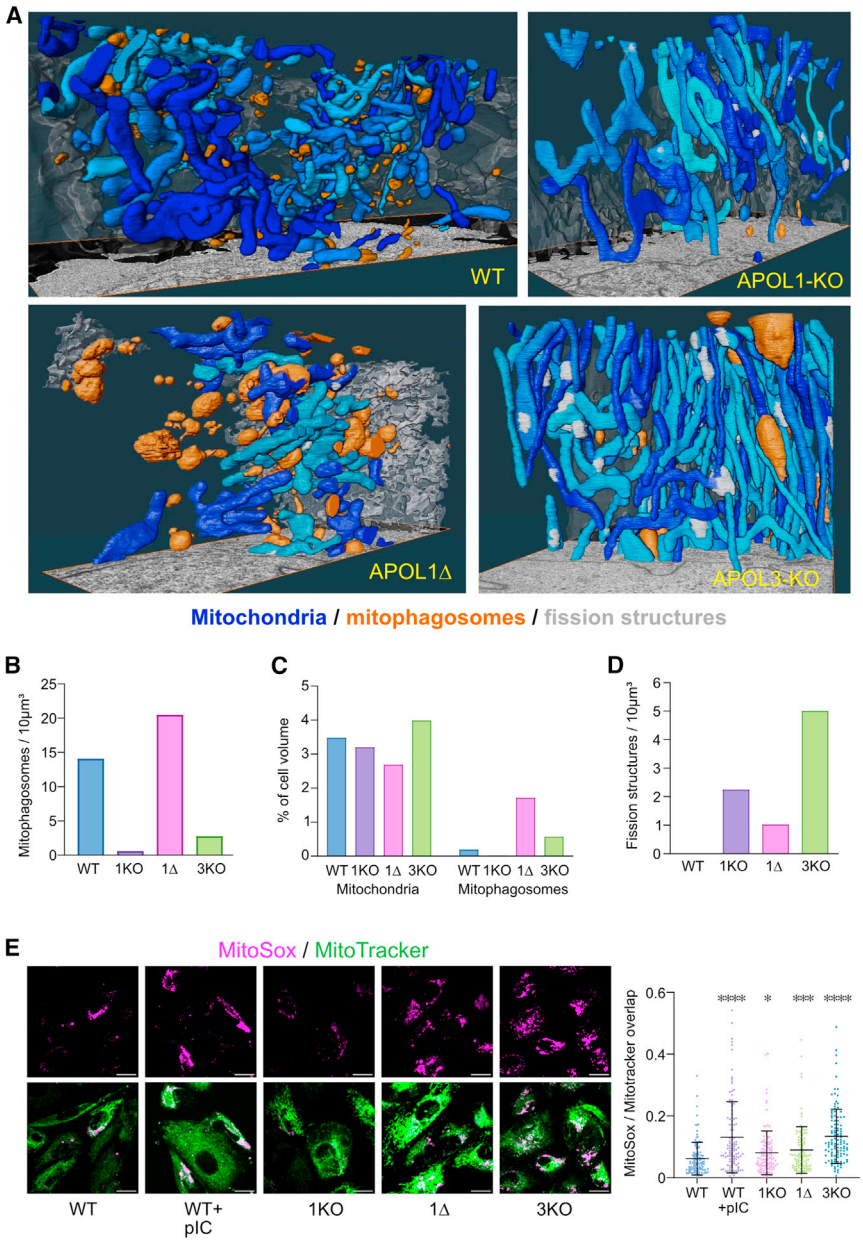

Figure 5. Effects of APOL1/-3 gene editing on the morphology and activity of mitochondria

(A) FIB-SEM images of reconstructed 3D cell segments in various podocyte cell lines. Blue, mitochondria; orange, mitophagosomes; light gray, unresolved fission structures; dark gray, cytoplasm or cytoplasmic membrane. Videos are provided at https://owncloud.ulb.ac.be/index.php/s/pkny92qwROGq1df.

(B) Number of mitophagosomes per 10 μm^3 for the segments shown in (A).

(C) Volumes of mitochondria and mitophagosomes for the segments shown in (A), expressed as percentages of cell volumes.

(D) Number of structures showing unresolved mitochondrial fission for the segments shown in (A).

(E) Live measurement of mitochondrial ROS production in various podocyte cell lines, as determined by co-localization of MitoSox and MitoTracker staining. Bars: 20 μm. n = 3; Mann-Whitney test, *p < 0.05; ***p < 0.001; ****p < 0.0001. Error bars represent the standard deviation.

murine cells.[81] PHB2 is a mitophagy receptor involved in the IFN inflammatory response.[37,82,83]

pDUET interaction assays in *Escherichia coli* revealed the binding of APOL1, but not APOL3, to PHB2 (Figure 6A). Although PHB2 peptides were detected by mass spectrometry in APOL1 immunoprecipitates of podocyte extracts,[11] PHB2 could not be observed in western blots of these immunoprecipitates, suggesting that *in vivo*, only a minor fraction of APOL1 could interact with PHB2. APOL1-PHB2 interaction did not involve LZs since it was unaffected by APOL1 LZ2 deletion (in APOL1Δ) or mutation of key LZ1 leucines (in APOL1 MutHel4Q) (Figures 6A and S6A).

Antiparallel homodimerization of a coiled coil in the PHB2 C-terminal region (A210-L242) provides a scaffold for organizing mitochondrial membrane complexes through interactions mediated by a cluster of negatively charged residues.[84] In APOL1, the N-terminal domain contains a positively charged helix (helix 5) with a sequence resembling the apoptotic motif BCL homology-3 (BH3).[26] The positively charged residues of helix 5 face the negatively charged residues on the PHB2 double helix (Figure S6B). In SPR assays, both APOL1 and APOL3 helix 5 peptides exhibited Ca^{2+}-dependent binding to PHB2 (Figure 6B). This interaction likely occurred through coiled coiling (Figure S6B). Helix 5 also homodimerized and interacted with the APOL3 C-terminal domain (Figure 6C), likely through coiled coiling with LZ2 (Figure S2B). Neither helix 5 hydrophobicity reduction (in mutHel5Q: Figure S6A) nor helix 5 disruption (in mutHel5P: Figure S6A) abolished APOL1 interaction with PHB2 (Figure 6A). Furthermore, neither neutralizing the positive charges in helix 5 (H5S: Figure S6B) nor introducing negative charges in the BH3-like motif (BH3E: Figure S6B), which inactivates BH3 in mice,[85] reduced PHB2 binding to APOL1 (Figure 6A). Similarly, converting the sequence of the helix 4–5 linker loop of APOL1 into the highly divergent one of APOL3 (Figure S6A) did not affect APOL1-PHB2 interaction (Figure 6A).

In conclusion, the specific binding of PHB2 to APOL1 may involve Ca^{2+}-dependent interaction with helix 5, but it does not result from exposure of positive residues or hydrophobic heptad repeats in helix 5. APOL1 interaction with PHB2 may target the

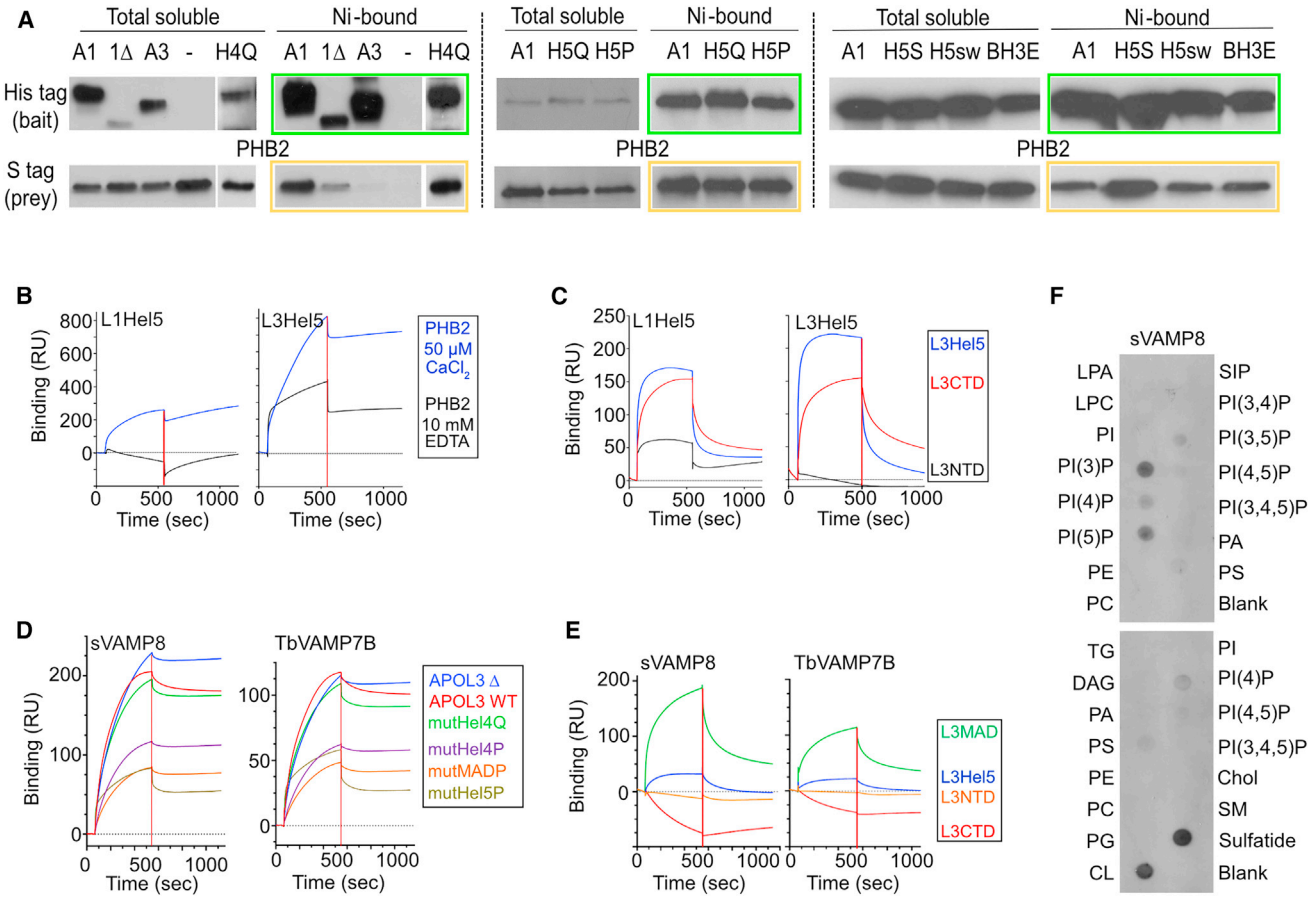

Figure 6. APOL1- and APOL3-specific interactions

(A) Interaction of APOL1, APOL1 mutants, or APOL3 with PHB2, as measured in the *E. coli* pDUET co-expression system. Nickel binding of S-tagged proteins (yellow frame) reflects their relative association with His-tagged partners (green frame). These data are representative of at least 3 independent experiments. A1, WT APOL1; Δ, APOL1Δ; A3, WT APOL3; H4Q, APOL1 mutHel4Q; H5Q, APOL1 mutHel5Q; H5P, APOL1 mutHel5P; H5mS, APOL1 mutHel5S; H5sw, APOL1 Hel5 swap; BH3E, APOL1 BH3 mutant E.

(B) Representative SPR sensorgrams of immobilized L1Hel5 (left) or L3Hel5 (right) peptide interaction with recombinant PHB2 with or without calcium (n = 3).

(C) Representative SPR sensorgrams of immobilized L1Hel5 (left) or L3Hel5 (right) peptide interaction with APOL3 Hel5, NTD, or CTD peptide (n = 3).

(D) SPR measurements of bound sVAMP8 (left) or TbVAMP7Bp (right) interaction with various APOL3 versions as indicated (n = 3).

(E) SPR measurements of bound sVAMP8 (left) or TbVAMP7Bp (right) interaction with different APOL3 peptides as indicated (n = 3).

(F) Immunodetection of recombinant sVAMP8 binding to various lipids spotted on membrane strips. LPA, lysophosphatidic acid; LPC, lysophosphocholine; PI, phosphatidylinositol; PE, phosphatidylethanolamine; PC, phosphatidylcholine; S1P, sphingosine-1-phosphate; PA, phosphatidic acid; PS, phosphatidylserine; TG, triglyceride; DAG, diacylglycerol; PG, phosphatidylglycerol; CL, cardiolipin; Chol, cholesterol; SM, sphingomyelin. Blank, no lipid.

APOL3-PI4KB complex to MERCSs for initiation of mitochondrial membrane fission and mitophagy.

APOL3 interacts with the R-SNARE protein VAMP8

In vitro, the APOL1 C-terminal domain can interact with vesicle-associated membrane protein-8 (VAMP8),[86] and in trypanosomes, a VAMP8 homolog (TbVAMP7B: Tritryp Tb927.5.3560) is involved in APOL1 trypanolytic activity.[87] Consistently, APOL3 interacted with both soluble VAMP8 (sVAMP8; M1–M76 region) and the R-SNARE helix of TbVAMP7B (Figure 6D).

SNARE-mediated membrane fusion requires coiling of four helices (SNARE domains) located near transmembrane domains.[88,89] We investigated the possible interaction of VAMP8 with different APOL3 helices with coiling potential (Figure S6C), including the "membrane-addressing domain" (MAD),[13] a double-stranded helix (MAD1-2) near the transmembrane hairpin. APOL3 interaction with VAMP8 was not driven by LZs because either LZ2 deletion or mutation of key LZ1 leucines conserved full APOL3 interaction with either sVAMP8 or TbVAMP7B peptides (Figure 6D). Helices 4–5, MAD1-2, and HC2-LZ2 primarily fold in hairpins but also exhibit a SNARE-like structure (Figures S6E and S6F). Only the APOL3 helices 5 and MAD1-2 bound to the sVAMP8 or TbVAMP7B peptide (Figure 6E), and proline-driven disruption of helix 4 or 5 or MAD1-2 reduced this interaction (Figure 6D). Thus, APOL3 interaction with either sVAMP8 or TbVAMP7B appeared to involve more than a single helix. *In silico* modeling predicted that upon interaction with either helices 4–5 or MAD1-2, the VAMP8 helix can fold into a hairpin, generating SNARE-like four-helix bundles (Figure S6F).

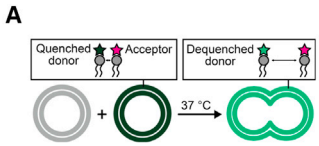

B

Protein	Lipids (mol %) P : L	PC	PS	Chol	PE	SM	PI	CL	N-PE	R-PE
VAMP8	800	27	2	30	17	15	6	---	1.5	1.5
APOL1/3	1000	33 (55)	2	---	30	---	13	22 (0)	---	---

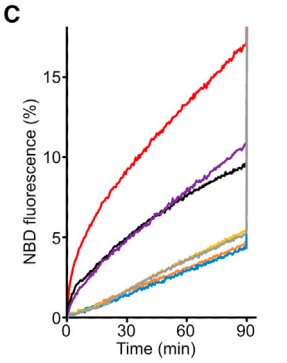

SUV	N/R-SUV	Additive	n	std
APOL3	VAMP8	---	4	3,76
APOL3	---	---	3	0,53
APOL3	VAMP8	+sVAMP8	3	0,58
APOL3	VAMP8	- CL	5	3,67
APOL3	VAMP8	+sVAMP8 -CL	3	0,46
APOL1	VAMP8	---	3	0,42
APOL1	VAMP8	pH5, then pH7	3	0,40

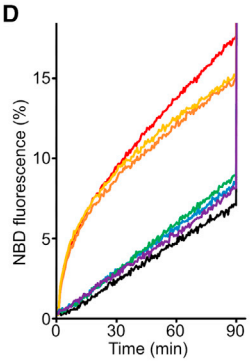

SUV	N/R-SUV	n	std
APOL3	VAMP8	4	3,76
APOL3Δ	VAMP8	3	1,78
mutHel4Q	VAMP8	3	2,79
mutHel4P	VAMP8	3	2,83
mutHel5Q	VAMP8	4	2,36
mutHel5P	VAMP8	4	2,64
mutMADP	VAMP8	4	2,68

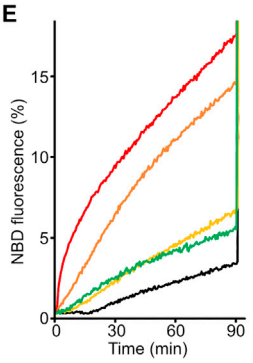

SUV	N/R-SUV	Additive	n	std
APOL3	VAMP8	---	4	3,76
Q-SNARE	VAMP8	---	2	0,47
Q-SNARE	VAMP8	+sVAMP8	2	0,53
Q-SNARE	APOL3	---	2	1,15
Q-SNARE	---	---	2	0,12

Figure 7. Vesicular membrane fusion induced by APOL3 and VAMP8

(A) Scheme of the lipid mixing assay. The fluorescence of the donor dye (NBD, dark green star) quenched due to the proximity to the acceptor dye (rhodamine, pink star) is increased upon membrane fusion with non-fluorescent partner SUVs.

(B) Protein and lipid composition of small unilamellar vesicles (SUVs) involved in the fusion assays. P:L, protein:lipid ratio; N-PE, NBD-PE; R-PE, rhodamine-PE (see STAR Methods for lipid abbreviations). In red, alternative lipid composition ("-CL" condition).

(C) Fusion assays between APOL3 or APOL1 SUVs and VAMP8 N/R (N-PE/R-PE) SUVs (n = number of replicates; SD = standard deviation at t = 90).

(D) Same as in (C) but including SUVs with APOL3 mutants.

(E) Same as in (C) but including SUVs with STX1A + SNAP25.

Finally, like APOL1 and APOL3,[11] sVAMP8 bound to cardiolipin (Figure 6F), suggesting that the APOL3/VAMP8 fusogenic activity involves cardiolipin.[28]

Together with VAMP8, APOL3 promotes fusion between vesicular liposomes

The endosomal protein VAMP8 is the only SNARE known to be required for mitophagy. The Q-SNAREs syntaxin-17 (STX17) and synaptosome-associated protein-29 (SNAP29), involved in autophagosome-endolysosome fusion,[90] are dispensable in this process.[91,92] In liposomes containing mitochondrial lipids, APOL3, but not APOL1, promoted vesicle fusion with VAMP8-carrying liposomes made of endosomal-like membranes, and the absence of cardiolipin reduced this fusion (Figures 7A–7C). Conferring transmembrane insertion of APOL1 by preincubation at pH 5 promoted its fusion activity at neutral pH, albeit less efficiently than APOL3 (Figure 7C). Both interactions with sVAMP8 and transmembrane anchoring of VAMP8 were necessary for this fusion because either VAMP8 absence or addition of sVAMP8 prevented it (Figure 7C). Reduction of helix 4 hydrophobicity or LZ2 deletion only mildly reduced APOL3 fusion activity, whereas disruption of helix 4 or 5 or MAD1-2 by proline insertions led to stronger reduction (Figure 7D). These results confirmed those of the APOL3-sVAMP8 interaction assays, indicating that more than one APOL3 helix is involved in fusion.

Finally, the APOL3 fusion activity was not observed with Q-SNARE-bearing liposomes (STX1A + SNAP25), and this activity was more efficient than that occurring between STX1A + SNAP25 and VAMP8 liposomes (Figure 7E).

We propose that in mitophagy, APOL3 helices 4–5 and MAD1-2 replace the STX17-SNAP29 helices involved in autophagosome-endolysosome fusion (Figures S6D and S7).

DISCUSSION

We report that APOL3 controls the key mitophagy processes of mitochondrial membrane fission and fusion through the respective APOL3 interactions with PI4KB and VAMP8.

APOL3 controls PI4KB activity at the Golgi

In addition to Ca^{2+}-dependent APOL3 interaction with NCS1,[11] APOL3 directly interacts with the N-terminal regulatory domain of PI4KB and forms a trimeric complex with PI4KB and NCS1, mimicking the complex between ARF1, PIK1, and FRQ1 in yeast.[65] Moreover, without Ca^{2+}, APOL3 interacted with CALN1, which is specifically involved in inactivating PI4KB at low Ca^{2+} concentrations.[57] *In vitro,* CALN1 inhibited PI4KB independently of APOL3, and in the presence of Ca^{2+}, APOL3 activated PI4KB independently of NCS1. PI4KB activation by APOL3 is likely relevant *in vivo* given the reduced Golgi PI4KB activity in APOL3-KO podocytes. Thus, *in vivo,* APOL3 may be involved in NCS1-Ca^{2+} recruitment to the Golgi membrane to reach the local Ca^{2+} concentration needed for PI4KB stimulation by APOL3. Whereas NCS1 exhibits extensive structural and functional similarities with yeast FRQ1,[59] there is no identified APOL homolog in yeast, suggesting that either FRQ1 activates PIK1 directly or FRQ1 binds to a lipoprotein with APOL-like helices.

Because NCS1, PI4KB, and actomyosin control secretion and exocytosis,[19,93,94] APOL3 is presumably involved in these processes. Accordingly, APOL3 inactivation or deletion resulted in important Golgi and actomyosin reorganization.[11]

APOL1Δ triggers APOL3 dissociation from PI4KB

APOL3 and APOL1 differ in that APOL3, but not APOL1, interacts with PI4KB. However, in contrast to APOL1, APOL1Δ interacted with PI4KB with high affinity. This interaction was stronger than that of APOL3, likely owing to the higher coiling potential of APOL1Δ HC1 over APOL3 HC1. Consequently,

APOL1Δ may trigger dissociation of APOL3 from PI4KB, possibly releasing PI4KB from anchoring to the Golgi membrane because, like WT APOL1, APOL1Δ cannot insert into membranes at neutral pH and does not bind to NCS1. This may explain the APOL1Δ-specific delocalization of APOL3 from PI4KB.[11] Such delocalization was not observed in G1 or G2 podocytes, consistent with the only weak G1/G2 interaction with PI4KB. In all three cases, PI4KB activity was reduced[11] but at a higher level in APOL1Δ cells, probably explaining the higher dysfunction severity in these cells. APOL1Δ-mediated APOL3 dissociation from PI4KB may inactivate PI4KB like occurs following APOL3 deletion.

IFN-I signaling may interfere with APOL3-PI4KB interaction

Under virus-induced inflammation, PI4KB is trafficked from the Golgi to the PAS, where PI4KB activity is required for auto-/mitophagy induction.[40,41,44,45,73] We found that the PI4KB helices that can interact with APOL3 bound to an ARF1 peptide (S93-H145) are also able to strongly interact with APOL3. Moreover, recombinant ARF1 interacted *in vitro* with APOL3 but not with PI4KB. Therefore, ARF1 interaction with PI4KB and APOL3 may be mutually exclusive. IFN-I signaling promotes ARF1 activation (GTP binding), which allows ARF1 membrane anchoring and enhanced ARF1 binding to PI4KB. Thus, like APOL1Δ, IFN-I signaling may interfere with APOL3-PI4KB interaction. However, unlike APOL1Δ, IFN-I neither dissociates nor inactivates APOL3 and PI4KB.

Interference with APOL3 activity promotes PI4KB delocalization

PI4KB dissociation from APOL3 in APOL3-KO and APOL1Δ cells is linked to reduced PI4KB activity at the Golgi and increased numbers of MERCS structures. MERCS numbers increase upon autophagy induction.[95] To trigger autophagy, PI4KB is trafficked in Golgi-derived ATG9A vesicles,[40] which also carry APOL3 and APOL1. Thus, PI4KB dissociation from APOL3 may trigger both PI4KB trafficking from the Golgi and increased MERCS formation, associated with auto-/mitophagy induction. Accordingly, the ATG9A coalescence in APOL3-KO and APOL1Δ cells may be related to autophagy because ATG9A vesicle coalescence occurs at the PAS when autophagy is initiated.[68,96–98]

PI4KB and APOL3 delocalization involves APOL1

Several observations support the involvement of APOL1 in APOL3/PI4KB trafficking from the Golgi to MERCSs. (1) APOL1 is found with PI4KB in APOL3 immunoprecipitates.[11] (2) APOL1 strongly co-localizes with ATG9A vesicles that traffic PI4KB from the Golgi to the PAS.[40] (3) APOL1 can directly associate with mitochondria.[26,27] (4) In APOL1-KO cells, the mitochondrial fission rate is decreased, suggesting that APOL1 absence lowers PI4KB targeting to the mitochondria. (5) In APOL1-KO cells, mitophagosome-endolysosome fusion and poly(I:C)-induced apoptosis are reduced,[11] suggesting that APOL1 absence lowers APOL3 targeting to the mitochondria. (6) In APOL1+3-KO cells, the mitochondrial phenotype due to APOL3 deletion is reverted,[11] confirming the role of APOL1 in PI4KB targeting to the mitochondria. (7) APOL1 binding to PHB2 may hypothetically allow PI4KB association with MERCSs, which are both interacting sites for mitophagy receptors and mitochondrial fission sites,[77] and the calcium dependence of APOL1-PHB2 interaction may relate to the NCS1-driven Ca^{2+} accumulation at MERCSs.[99–101]. (8) APOL3/PI4KB traffic could involve the tight APOL1 association with NM2A, the myosin responsible for ATG9A vesicle transport.[11,38,40,41]

Interference with APOL3 activity reduces both fission and fusion of mitochondrial membranes

The mitophagosome accumulation in APOL1Δ and APOL3-KO cells was not due to eventual induction of IFN-I signaling because in both cases, the typical IFN-I-linked increase in APOL1 expression occurred only when poly(I:C) was added.[11] In these cells, the accumulation of both unresolved mitochondrial budding structures and enlarged mitophagosomes strongly suggests that APOL3 absence or inactivation affects both membrane fission and fusion. Given the differential accumulation of unresolved fission and fusion structures in APOL3-KO and APOL1Δ cells, respectively, APOL3 absence likely affects mostly mitochondrial membrane fission, whereas APOL3 inactivation by APOL1Δ mostly affects mitophagosome-endolysosome fusion. Fission reduction in APOL3-KO cells explains the lower accumulation of mitophagosomes compared to that of APOL1Δ cells, where fission is less affected.

Interference with APOL3 activity may affect PI4KB-mediated fission of mitochondrial membranes

Because APOL3 controls PI4KB activity, the decreased fission rate in APOL3-KO cells likely results from PI4KB inactivation, affecting the mitophagy flux at its initial stage. Indeed, PI4KB is involved in both mitochondrial membrane fission and initiation of autophagy,[20,40,102–104] and mitochondrial fission is linked to mitophagy induction.[105] Consistently, depletion of the PI4KB product PI(4)P at the mitochondrial division site inhibits fission.[106] PI(4)P favors membrane recruitment of the fission factor NM2A and associated membrane-bending factors[107,108] and is linked to actin polymerization at the fission site.[109] PI(4)P recruits Golgi phosphoprotein-3 (GOLPH3), a PHB2-associated *trans*-Golgi and mitochondrial protein that binds to the F-actin and NM2A binder myosin-18A, generating a pulling force for membrane fission.[37,110–112] At the mitochondrial membrane, lipid-raft-like domains are involved in recruiting fission factors such as FIS1 and dynamin-related protein-1 (DRP1) together with STX17.[20,113–116] Because mitophagy depends on membrane fission independently of DRP1,[105,117] the role of PI4KB in mitophagy could be the organization of PI(4)P-enriched rafts allowing recruitment of fission factors distinct from DRP1. A clear candidate is FIS1, involved in stress-induced fission and mitophagy,[118] which may oligomerize at lipid rafts through its ability to bind anionic phospholipids.[119] Interestingly, in APOL3-KO and at a lower level in APOL1Δ cells, the co-localization between PI4KB and FIS1 was increased.

Therefore, synthesis of PI(4)P by PI4KB is crucial for membrane fission, and distribution of this fission between the Golgi and mitochondria likely depends on APOL3 and APOL1, respectively.

Interference with APOL3 activity reduces mitophagosome fusion with endolysosomes

Accumulation of enlarged mitophagosomes in APOL1Δ cells is linked to impaired mitophagosome-endolysosome fusion. Similarly, the autophagic flux is reduced in G1- or G2-expressing mice,[120] consistent with inhibition of mitophagosome-endolysosome fusion. This fusion activity is likely due to APOL3. Indeed, APOL3 interacts with the fusogenic R-SNARE protein VAMP8, and together, these proteins promoted vesicular membrane fusion *in vitro*. Two APOL3 helix tandems (helices 4–5 and MAD1-2) contribute to this interaction (model in Figure S7). Modeling predicted that the SNARE helix of VAMP8 can fold into a hairpin when interacting with each APOL3 helix tandem, generating SNARE-like four-helix bundles.

STX17 was identified as a partner of VAMP8 for autophagosome-endolysosome fusion.[90] However, the SNARE partner(s) of VAMP8 for mitophagosome-endolysosome fusion remained unknown.[92] APOL3 may fulfill this function. In both STX17 and APOL3, membrane anchoring is ensured by a double-stranded hairpin with high flexibility, as measured by the high proportion of β-branched (Ile/Val) and helix-breaking (Gly/Pro/Ser/Thr) amino acids in the two membrane spans of the hairpin (total 12/21 and 12/21 for STX17 and 16/24 and 15/24 for APOL3). Such flexibility is also characteristic of the VAMP8 and FIS1 C-terminal helices (13/24 and 14/26, respectively). Hydrophobic helix flexibility is crucial for transmembrane peptides to drive membrane fusion[88] and may explain the detergent-like activity of APOL3 on bacterial membranes.[29] Additional similarities between STX17 and APOL3 include Golgi-to-mitochondrion trafficking and activity in both mitochondrial fission and auto-/mitophagy initiation.[115,116,121,122]

The role of APOL3 in mitophagy may relate to its binding activity to cardiolipin,[11] which is incorporated in the mitophagosome membrane.[123–126] Thus, APOL3 may be targeted to the mitophagosome membrane. Moreover, VAMP8 also binds to cardiolipin. APOL3 and VAMP8 binding to cardiolipin may explain the promoting effect of cardiolipin on their fusogenic activity. Accordingly, the detergent-like activity of APOL3 on cardiolipin-rich membranes of intracellular bacteria[29] may require association with VAMP8 for bacterial degradation in endolysosomes.

In contrast to APOL3, APOL1 exhibited no fusogenic activity despite its capacity to bind VAMP8, likely because APOL1 requires low pH for transmembrane insertion.[14] Incubation with liposomes at low pH was sufficient to confer fusogenic activity to APOL1, as occurs in trypanosomes where APOL1 transit in acidic endosomes promotes fusion between mitochondrial membranes, which is also observed with APOL3.[26] Because a trypanosome homolog of VAMP8 (TbVAMP7B) is involved in APOL1 trypanolytic activity,[87] TbVAMP7B may promote the fusion between APOL1-carrying endosomes and the mitochondrion.

Interference with APOL3 activity inhibits apoptosis

APOL activities on mitochondrial dynamics may also account for their apoptotic activity, both in trypanosomes and human cells.[11,26,31,127] The specific fusogenic activity of APOL3 appears to be involved in apoptosis because in APOL3-KO cells, poly(I:C)-induced apoptosis was inhibited despite the presence of APOL1.[11]

Interference with APOL3 activity results in mitochondrion-dependent cellular damage

Upon APOL3 absence or APOL3 interaction with APOL1Δ, incomplete mitophagy prevented digestion of damaged mitochondria, triggering generation of mitochondrial ROS, which also occurs in the presence of poly(I:C). Moreover, in APOL1Δ podocytes, poly(I:C)-induced apoptosis nearly disappeared,[11] allowing persistence of cells with dysfunctional mitochondria. Finally, interference with nuclear PI4KB activity may also affect mitochondrial functions by altering mRNA levels, as observed for NCS1 deficiency.[25] Given the phenotypic similarities between APOL1Δ and G1/G2 podocytes,[11] G1/G2 cells likely share this pathology, albeit less severely. Accordingly, APOL1 G1/G2 expression triggers mitochondrial dysfunctions,[51] inducing exacerbated sepsis[128] or hypertension.[129] Because kidney function is particularly affected by interference with mitochondrial fission,[130] altered mitochondrial membrane dynamics could account for the nephropathy in patients expressing G1 or G2 (HIVAN and COVAN: HIV- and COVID-19-associated nephropathy, respectively).[8]

Conclusions

Because APOL3 interacts with both fission and fusion factors, it may control membrane dynamics in different organelles, such as the Golgi and mitochondria, and may be involved in secretion, exocytosis, and auto-/mitophagy.

We propose the following scheme for APOL involvement in mitophagy induced by poly(I:C) (Figure S7): (1) poly(I:C)-mediated disruption of APOL3-PI4KB interaction at the Golgi via activation of ARF1; (2) trafficking of PI4KB/ARF1 and APOL3/NCS1 to MERCSs owing to APOL1 association with NM2A and PHB2; (3) involvement of PI4KB/ARF1 in mitochondrion fission; and (4) involvement of APOL3/VAMP8 in mitophagosome-endolysosome fusion.

APOL3 deletion or APOL3 inactivating interaction with APOL1 C-terminal variants mimics poly(I:C) in triggering PI4KB delocalization from the Golgi to MERCSs. However, the reduced rate of fission due to PI4KB inactivation (especially in APOL3-KO) and the reduced rate of fusion due to APOL3 inactivation (especially in APOL1Δ) cause decreased mitophagy flux and consecutive pathology.

Limitations of the study

We could not generate experimental G1 or G2 podocytes via CRISPR-Cas9-mediated gene editing. Thus, we could not compare them with the other CRISPR-Cas9-edited cell lines (APOL1-KO, APOL3-KO, and APOL1Δ).

STAR★METHODS

Detailed methods are provided in the online version of this paper and include the following:

- KEY RESOURCES TABLE
- RESOURCE AVAILABILITY
  - Lead contact and materials availability
  - Materials availability
  - Data and code availability

SUPPLEMENTAL INFORMATION

Supplemental information can be found online at https://doi.org/10.1016/j.celrep.2023.113528.

ACKNOWLEDGMENTS

We acknowledge the excellent technical assistance of S.M. Andersen (Odense, Denmark) and Marjorie Vermeersch (CMMI). This work was supported by the European Research Council (ERC) grant 669007-APOLs (to E.P.); the Action de Recherches Concertées of the University of Brussels (ULB, ARC ADV, to D.P.-M.); the Belgian Fonds de la Recherche Scientifique (FNRS) grant T.0178.21 (to D.P.-M.); the Agence Nationale de la Recherche grant ANR-20-ERC9-0002 (to P.H.); and the Danish National Research Foundation (grant DNRF141) to the Center for Functional Genomics and Tissue Plasticity (ATLAS). The CMMI is supported by the European Regional Development Fund and the Walloon Region.

AUTHOR CONTRIBUTIONS

L.L. generated all WT and mutant recombinant proteins and performed the immunofluorescence analyses, PI4KB activity assays, and pDUET measurements; P.H. and F.P. performed the vesicle fusion assays; J.H.G., D.H., and M.K.S. performed the protein and peptide binding assays; A.C.d'E. and D.P.-M. performed the FIB-SEM analyses; and E.P. conceived the work and wrote the manuscript.

DECLARATION OF INTERESTS

The authors declare no competing interests.

Received: July 12, 2023
Revised: November 8, 2023
Accepted: November 17, 2023

REFERENCES

1. Pays, E. (2021). The function of Apolipoproteins L (APOLs): relevance for kidney disease, neurotransmission disorders, cancer and viral infection. FEBS J. *288*, 360–381.
2. Vanhamme, L., Paturiaux-Hanocq, F., Poelvoorde, P., Nolan, D.P., Lins, L., Van Den Abbeele, J., Pays, A., Tebabi, P., Van Xong, H., Jacquet, A., et al. (2003). Apolipoprotein L-I is the trypanosome lytic factor of human serum. Nature *422*, 83–87.
3. Pays, E., Vanhollebeke, B., Uzureau, P., Lecordier, L., and Pérez-Morga, D. (2014). The molecular arms race between African trypanosomes and humans. Nat. Rev. Microbiol. *12*, 575–584.
4. Genovese, G., Friedman, D.J., Ross, M.D., Lecordier, L., Uzureau, P., Freedman, B.I., Bowden, D.W., Langefeld, C.D., Oleksyk, T.K., Uscinski Knob, A.L., et al. (2010). Association of trypanolytic ApoL1 variants with kidney disease in African Americans. Science *329*, 841–845.
5. Kopp, J.B., Heymann, J., and Winkler, C.A. (2017). APOL1 renal risk variants: fertile soil for HIV-associated nephropathy. Semin. Nephrol. *37*, 514–519.
6. Beckerman, P., and Susztak, K. (2018). APOL1: The balance imposed by infection, selection, and kidney disease. Trends Mol. Med. *24*, 682–695.
7. Friedman, D.J., and Pollak, M.R. (2020). APOL1 and kidney disease: From genetics to biology. Annu. Rev. Physiol. *82*, 323–342.
8. Velez, J.C.Q., Caza, T., and Larsen, C.P. (2020). COVAN is the new HIVAN: the re-emergence of collapsing glomerulopathy with COVID-19. Nat. Rev. Nephrol. *16*, 565–567.
9. Pays, E. (2020). The mechanism of kidney disease due to APOL1 risk variants. J. Am. Soc. Nephrol. *31*, 2502–2505.
10. Bruggeman, L.A., Sedor, J.R., and O'Toole, J.F. (2021). Apolipoprotein L1 and mechanisms of kidney disease susceptibility. Curr. Opin. Nephrol. Hypertens. *30*, 317–323.
11. Uzureau, S., Lecordier, L., Uzureau, P., Hennig, D., Graversen, J.H., Homblé, F., Mfutu, P.E., Oliveira Arcolino, F., Ramos, A.R., La Rovere, R.M., et al. (2020). APOL1 C-terminal variants may trigger kidney disease through interference with APOL3 control of actomyosin. Cell Rep. *30*, 3821–3836.e13.
12. Daneshpajouhnejad, P., Kopp, J.B., Winkler, C.A., and Rosenberg, A.Z. (2022). The evolving story of apolipoprotein L1 nephropathy: the end of the beginning. Nat. Rev. Nephrol. *18*, 307–320.
13. Pérez-Morga, D., Vanhollebeke, B., Paturiaux-Hanocq, F., Nolan, D.P., Lins, L., Homblé, F., Vanhamme, L., Tebabi, P., Pays, A., Poelvoorde, P., et al. (2005). Apolipoprotein L-I promotes trypanosome lysis by forming pores in lysosomal membranes. Science *309*, 469–472.
14. Fontaine, F., Lecordier, L., Vanwalleghem, G., Uzureau, P., Van Reet, N., Fontaine, M., Tebabi, P., Vanhollebeke, B., Büscher, P., Pérez-Morga, D., and Pays, E. (2017). APOLs with low pH dependence can kill all African trypanosomes. Nat. Microbiol. *2*, 1500–1506.
15. Skorecki, K.L., Lee, J.H., Langefeld, C.D., Rosset, S., Tzur, S., Wasser, W.G., Shemer, R., Hawkins, G.A., Divers, J., Parekh, R.S., et al. (2018). A null variant in the apolipoprotein L3 gene is associated with non-diabetic nephropathy. Nephrol. Dial. Transplant. *33*, 323–330.
16. Gromada, J., Bark, C., Smidt, K., Efanov, A.M., Janson, J., Mandic, S.A., Webb, D.L., Zhang, W., Meister, B., Jeromin, A., and Berggren, P.-O. (2005). Neuronal calcium sensor-1 potentiates glucose-dependent exocytosis in pancreatic beta cells through activation of phosphatidylinositol 4-kinase beta. Proc. Natl. Acad. Sci. USA *102*, 10303–10308.
17. Korobova, F., Gauvin, T.J., and Higgs, H.N. (2014). A role for myosin II in mammalian mitochondrial fission. Curr. Biol. *24*, 409–414.
18. Miserey-Lenkei, S., Bousquet, H., Pylypenko, O., Bardin, S., Dimitrov, A., Bressanelli, G., Bonifay, R., Fraisier, V., Guillou, C., Bougeret, C., et al. (2017). Coupling fission and exit of RAB6 vesicles at Golgi hotspots through kinesin-myosin interactions. Nat. Commun. *8*, 1254.
19. Waugh, M.G. (2019). The great escape: How phosphatidylinositol4-kinases and PI4P promote vesicle exit from the Golgi (and drive cancer). Biochem. J. *476*, 2321–2346.
20. Nagashima, S., Tábara, L.C., Tilokani, L., Paupe, V., Anand, H., Pogson, J.H., Zunino, R., McBride, H.M., and Prudent, J. (2020). Golgi-derived PI(4)P-containing vesicles drive late steps of mitochondrial division. Science *367*, 1366–1371.
21. de Graaf, P., Klapisz, E.E., Schulz, T.K.F., Cremers, A.F.M., Verkleij, A.J., and van Bergen en Henegouwen, P.M.P. (2002). Nuclear localization of phosphatidylinositol 4-kinase beta. J. Cell Sci. *115*, 1769–1775.

22. Strahl, T., Hama, H., DeWald, D.B., and Thorner, J. (2005). Yeast phosphatidylinositol 4-kinase, Pik1, has essential roles at the Golgi and in the nucleus. J. Cell Biol. *171*, 967–979.

23. Szivak, I., Lamb, N., and Heilmeyer, L.M.G. (2006). Subcellular localization and structural function of endogenous phosphorylated phosphatidylinositol 4-kinase (PI4K92). J. Biol. Chem. *281*, 16740–16749.

24. Fáberová, V., Kalasová, I., Krausová, A., and Hozák, P. (2020). Super-resolution localisation of nuclear PI(4)P and identification of its interacting proteome. Cells *9*, 1191.

25. Simons, C., Benkert, J., Deuter, N., Poetschke, C., Pongs, O., Schneider, T., Duda, J., and Liss, B. (2019). NCS-1 deficiency affects mRNA levels of genes involved in regulation of ATP synthesis and mitochondrial stress in highly vulnerable substantia nigra dopaminergic neurons. Front. Mol. Neurosci. *12*, 252.

26. Vanwalleghem, G., Fontaine, F., Lecordier, L., Tebabi, P., Klewe, K., Nolan, D.P., Yamaryo-Botté, Y., Botté, C., Kremer, A., Burkard, G.S., et al. (2015). Coupling of lysosomal and mitochondrial membrane permeabilization in trypanolysis by APOL1. Nat. Commun. *6*, 8078.

27. Chidiac, M., Daher, J., Boeckstaens, M., Poelvoorde, P., Badran, B., Marini, A.M., Khalaf, R., and Vanhamme, L. (2020). Human apolipoprotein L1 interferes with mitochondrial function in *Saccharomyces cerevisiae*. Mol. Med. Rep. *22*, 1910–1920.

28. Kameoka, S., Adachi, Y., Okamoto, K., Iijima, M., and Sesaki, H. (2018). Phosphatidic acid and cardiolipin coordinate mitochondrial dynamics. Trends Cell Biol. *28*, 67–76.

29. Gaudet, R.G., Zhu, S., Halder, A., Kim, B.-H., Bradfield, C.J., Huang, S., Xu, D., Mamińska, A., Nguyen, T.N., Lazarou, M., et al. (2021). A human apolipoprotein L with detergent-like activity kills intracellular pathogens. Science *373*, eabf8113.

30. Nichols, B., Jog, P., Lee, J.H., Blackler, D., Wilmot, M., D'Agati, V., Markowitz, G., Kopp, J.B., Alper, S.L., Pollak, M.R., and Friedman, D.J. (2015). Innate Immunity pathways regulate the nephropathy gene Apolipoprotein L1. Kidney Int. *87*, 332–342.

31. Uzureau, S., Coquerelle, C., Vermeiren, C., Uzureau, P., Van Acker, A., Pilotte, L., Monteyne, D., Acolty, V., Vanhollebeke, B., Van den Eynde, B., et al. (2016). Apolipoproteins L control cell death triggered by TLR3/TRIF signaling in dendritic cells. Eur. J. Immunol. *46*, 1854–1866.

32. Schmeisser, H., Bekisz, J., and Zoon, K.C. (2014). New function of type I IFN: induction of autophagy. J. Interferon Cytokine Res. *34*, 71–78.

33. Hansen, M.D., Johnsen, I.B., Stiberg, K.A., Sherstova, T., Wakita, T., Richard, G.M., Kandasamy, R.K., Meurs, E.F., and Anthonsen, M.W. (2017). Hepatitis C virus triggers Golgi fragmentation and autophagy through the immunity-related GTPase M. Proc. Natl. Acad. Sci. USA *114*, E3462–E3471.

34. Zhang, L., Qin, Y., and Chen, M. (2018). Viral strategies for triggering and manipulating mitophagy. Autophagy *14*, 1665–1673.

35. Yi, C., Tong, J.-J., and Yu, L. (2018). Mitochondria: the hub of energy deprivation-induced autophagy. Autophagy *14*, 1084–1085.

36. Tian, Y., Wang, M.-L., and Zhao, J. (2019). Crosstalk between autophagy and type I Interferon responses in innate antiviral immunity. Viruses *11*, 132.

37. Wang, K., Qi, Y., Wang, X., Liu, Y., Zhao, M., Zhou, D., Zhang, Y., Wang, Y., Yu, R., and Zhou, X. (2021). GOLPH3 promotes glioma progression by enhancing PHB2-mediated autophagy. Am. J. Cancer Res. *11*, 2106–2123.

38. Tang, H.W., Wang, Y.B., Wang, S.L., Wu, M.H., Lin, S.Y., and Chen, G.C. (2011). Atg1-mediated myosin II activation regulates autophagosome formation during starvation-induced autophagy. EMBO J. *30*, 636–651.

39. Kruppa, A.J., Kendrick-Jones, J., and Buss, F. (2016). Myosins, actin and autophagy. Traffic *17*, 878–890.

40. Judith, D., Jefferies, H.B.J., Boeing, S., Frith, D., Snijders, A.P., and Tooze, S.A. (2019). ATG9A shapes the forming autophagosome through Arfaptin 2 and phosphatidylinositol 4-kinase IIIb. J. Cell Biol. *218*, 1634–1652.

41. De Tito, S., Hervás, J.H., van Vliet, A.R., and Tooze, S.A. (2020). The Golgi as an assembly line to the autophagosome. Trends Biochem. Sci. *45*, 484–496.

42. Delang, L., Paeshuyse, J., and Neyts, J. (2012). The role of phosphatidylinositol 4-kinases and phosphatidylinositol 4-phosphate during viral replication. Biochem. Pharmacol. *84*, 1400–1408.

43. Horner, S.M., Wilkins, C., Badil, S., Iskarpatyoti, J., and Gale, M. (2015). Proteomic analysis of mitochondrial-associated ER membranes (MAM) during RNA virus infection reveals dynamic changes in protein and organelle trafficking. PLoS One *10*, e0117963.

44. Altan-Bonnet, N. (2017). Lipid tales of viral replication and transmission. Trends Cell Biol. *27*, 201–213.

45. McPhail, J.A., and Burke, J.E. (2023). Molecular mechanisms of PI4K regulation and their involvement in viral replication. Traffic *24*, 131–145.

46. Lesage, S., Chazal, M., Beauclair, G., Batalie, D., Cerboni, S., Couderc, E., Lescure, A., Del Nery, E., Tangy, F., Martin, A., et al. (2022). Discovery of genes that modulate flavivirus replication in an interferon-dependent manner. J. Mol. Biol. *434*, 167277.

47. Hartleben, B., Gödel, M., Meyer-Schwesinger, C., Liu, S., Ulrich, T., Köbler, S., Wiech, T., Grahammer, F., Arnold, S.J., Lindenmeyer, M.T., et al. (2010). Autophagy influences glomerular disease susceptibility and maintains podocyte homeostasis in aging mice. J. Clin. Invest. *120*, 1084–1096.

48. Olasunkanmi, O.I., Chen, S., Mageto, J., and Zhong, Z. (2020). Virus-induced cytoplasmic aggregates and inclusions are critical cellular regulatory and antiviral factors. Viruses *12*, 399.

49. Ma, L., Ainsworth, H.C., Snipes, J.A., Murea, M., Choi, Y.A., Langefeld, C.D., Parks, J.S., Bharadwaj, M.S., Chou, J.W., Hemal, A.K., et al. (2020). APOL1 kidney-risk variants induce mitochondrial fission. Kidney Int. Rep. *5*, 891–904.

50. Blazer, A., Qian, Y., Schlegel, M.P., Algasas, H., Buyon, J.P., Cadwell, K., Cammer, M., Heffron, S.P., Liang, F.-X., Mehta-Lee, S., et al. (2022). APOL1 variant expressing endothelial cells exhibit autophagic dysfunction and mitochondrial stress. Front. Genet. *13*, 769936.

51. Ma, L., Palmer, N.D., Choi, Y.A., Murea, M., Snipes, J.A., Parks, J.S., Langefeld, C.D., and Freedman, B.I. (2020). APOL1 risk variants impair multiple mitochondrial pathways in a metabolomics analysis. Kidney360 *1*, 1353–1362.

52. Cho, D.H., Kim, J.K., and Jo, E.K. (2020). Mitophagy and innate immunity in infection. Mol. Cells *43*, 10–22.

53. Kohler, V., Aufschnaiter, A., and Büttner, S. (2020). Closing the gap: membrane contact sites in the regulation of autophagy. Cells *9*, 1184.

54. Wang, H., Zheng, Y., Huang, J., and Li, J. (2021). Mitophagy in antiviral immunity. Front. Cell Dev. Biol. *9*, 723108.

55. Li, Y., Wu, K., Zeng, S., Zou, L., Li, X., Xu, C., Li, B., Liu, X., Li, Z., Zhu, W., et al. (2022). The role of mitophagy in viral infection. Cells *11*, 711.

56. Sorouri, M., Chang, T., and Hancks, D.C. (2022). Mitochondria and viral infection: advances and emerging battlefronts. mBio *13*, e0209621–e0209622.

57. Mikhaylova, M., Reddy, P.P., Munsch, T., Landgraf, P., Suman, S.K., Smalla, K.-H., Gundelfinger, E.D., Sharma, Y., and Kreutz, M.R. (2009). Calneurons provide a calcium threshold for trans-Golgi network to plasma membrane trafficking. Proc. Natl. Acad. Sci. USA *106*, 9093–9098.

58. Daboussi, L., Costaguta, G., Ghukasyan, R., and Payne, G.S. (2017). Conserved role for Gga proteins in phosphatidylinositol 4-kinase localization to the trans-Golgi network. Proc. Natl. Acad. Sci. USA *114*, 3433–3438.

59. Strahl, T., Grafelmann, B., Dannenberg, J., Thorner, J., and Pongs, O. (2003). Conservation of regulatory function in calcium-binding proteins: human frequenin (neuronal calcium sensor-1) associates productively with yeast phosphatidylinositol 4-kinase isoform. J. Biol. Chem. *278*, 49589–49599.

60. Pandalaneni, S., Karuppiah, V., Saleem, M., Haynes, L.P., Burgoyne, R.D., Mayans, O., Derrick, J.P., and Lian, L.-Y. (2015). Neuronal Calcium Sensor-1 binds the D2 dopamine receptor and G-protein-coupled

receptor kinase 1 (GRK1) peptides using different modes of interactions. J. Biol. Chem. *290*, 18744–18756.

61. Strahl, T., Huttner, I.G., Lusin, J.D., Osawa, M., King, D., Thorner, J., and Ames, J.B. (2007). Structural insights into activation of phosphatidylinositol 4-kinase (Pik1) by yeast frequenin (Frq1). J. Biol. Chem. *282*, 30949–30959.
62. Godi, A., Pertile, P., Meyers, R., Marra, P., Di Tullio, G., Iurisci, C., Luini, A., Corda, D., and De Matteis, M.A. (1999). ARF mediates recruitment of PtdIns-4-OH kinase-beta and stimulates synthesis of PtdIns(4,5)P2 on the Golgi complex. Nat. Cell Biol. *1*, 280–287.
63. Haynes, L.P., Thomas, G.M.H., and Burgoyne, R.D. (2005). Interaction of neuronal calcium sensor-1 and ADP-ribosylation factor 1 allows bidirectional control of phosphatidylinositol 4-kinase b and trans-Golgi network-plasma membrane traffic. J. Biol. Chem. *280*, 6047–6054.
64. Haynes, L.P., Sherwood, M.W., Dolman, N.J., and Burgoyne, R.D. (2007). Specificity, promiscuity and localization of ARF protein interactions with NCS-1 and phosphatidylinositol-4 kinase-III beta. Traffic *8*, 1080–1092.
65. Highland, C.M., and Fromme, J.C. (2021). Arf1 directly recruits the Pik1-Frq1 PI4K complex to regulate the final stages of Golgi maturation. Mol. Biol. Cell *32*, 1064–1080.
66. Amor, J.C., Harrison, D.H., Kahn, R.A., and Ringe, D. (1994). Structure of the human ADP-ribosylation factor 1 complexed with GDP. Nature *372*, 704–708.
67. Ultsch, M., Holliday, M.J., Gerhardy, S., Moran, P., Scales, S.J., Gupta, N., Oltrabella, F., Chiu, C., Fairbrother, W., Eigenbrot, C., and Kirchhofer, D. (2021). Structures of the ApoL1 and ApoL2 N-terminal domains reveal a non-classical four-helix bundle motif. Commun. Biol. *4*, 916.
68. Yamamoto, H., Kakuta, S., Watanabe, T.M., Kitamura, A., Sekito, T., KondoKakuta, C., Ichikawa, R., Kinjo, M., and Ohsumi, Y. (2012). Atg9 vesicles are an important membrane source during early steps of autophagosome formation. J. Cell Biol. *198*, 219–233.
69. Maeda, S., Yamamoto, H., Kinch, L.N., Garza, C.M., Takahashi, S., Otomo, C., Grishin, N.V., Forli, S., Mizushima, N., and Otomo, T. (2020). Structure, lipid scrambling activity and role in autophagosome formation of ATG9A. Nat. Struct. Mol. Biol. *27*, 1194–1201.
70. Matoba, K., Kotani, T., Tsutsumi, A., Tsuji, T., Mori, T., Noshiro, D., Sugita, Y., Nomura, N., Iwata, S., Ohsumi, Y., et al. (2020). Atg9 is a lipid scramblase that mediates autophagosomal membrane expansion. Nat. Struct. Mol. Biol. *27*, 1185–1193.
71. Nishimura, T., and Tooze, S.A. (2020). Emerging Roles of ATG Proteins and Membrane Lipids in Autophagosome Formation. Cell Discovery *6*, 32.
72. Levine, B., Mizushima, N., and Virgin, H.W. (2011). Autophagy in immunity and inflammation. Nature *469*, 323–335.
73. Paul, P., and Münz, C. (2016). Autophagy and mammalian viruses: roles in immune response, viral replication, and beyond. Adv. Virus Res. *95*, 149–195.
74. Tresse, E., Riera-Ponsati, L., Jaberi, E., Sew, W.Q.G., Ruscher, K., and Issazadeh-Navikas, S. (2021). IFN-β rescues neurodegeneration by regulating mitochondrial fission via STAT5, PGAM5, and Drp1. EMBO J. *40*, e106868.
75. Le Vasseur, M., Chen, V.C., Huang, K., Vogl, W.A., and Naus, C.C. (2019). Pannexin 2 localizes at ER-Mitochondria Contact Sites. Cancers *11*, 343.
76. de Brito, O.M., and Scorrano, L. (2008). Mitofusin 2 tethers endoplasmic reticulum to mitochondria. Nature *456*, 605–610.
77. Friedman, J.R., Lackner, L.L., West, M., DiBenedetto, J.R., Nunnari, J., and Voeltz, G.K. (2011). ER tubules mark sites of mitochondrial division. Science *334*, 358–362.
78. Ziegler, D.V., Martin, N., and Bernard, D. (2021). Cellular senescence links mitochondria-ER contacts and aging. Commun. Biol. *4*, 1323.
79. Liu, L., Xie, R., Nguyen, S., Ye, M., and McKeehan, W.L. (2009). Robust autophagy/mitophagy persists during mitosis. Cell Cycle *8*, 1616–1620.
80. Murphy, M.P. (2009). How mitochondria produce reactive oxygen species. Biochem. J. *417*, 1–13.
81. Kreit, M., Vertommen, D., Gillet, L., and Michiels, T. (2015). The interferon-inducible mouse Apolipoprotein L9 and prohibitins cooperate to restrict Theiler's virus replication. PLoS One *10*, e0133190.
82. Giannotta, M., Fragassi, G., Tamburro, A., Vanessa, C., Luini, A., and Sallese, M. (2015). Prohibitin: a novel molecular player in KDEL receptor signalling. BioMed Res. Int. *2015*, 319454.
83. Wei, Y., Chiang, W.C., Sumpter, R., Jr., Mishra, P., and Levine, B. (2017). Prohibitin 2 is an inner mitochondrial membrane mitophagy receptor. Cell *168*, 224–238.e10.
84. Yoshinaka, T., Kosako, H., Yoshizumi, T., Furukawa, R., Hirano, Y., Kuge, O., Tamada, T., and Koshiba, T. (2019). Structural basis of mitochondrial scaffolds by prohibitin complexes: insight into a role of the coiled-coil region. iScience *19*, 1065–1078.
85. Wang, K., Gross, A., Waksman, G., and Korsmeyer, S.J. (1998). Mutagenesis of the BH3 domain of BAX identifies residues critical for dimerization and killing. Mol. Cell Biol. *18*, 6083–6089.
86. Madhavan, S.M., O'Toole, J.F., Konieczkowski, M., Barisoni, L., Thomas, D.B., Ganesan, S., Bruggeman, L.A., Buck, M., and Sedor, J.R. (2017). APOL1 variants change C-terminal conformational dynamics and binding to SNARE protein VAMP8. JCI Insight *2*, e92581.
87. Currier, R.B., Cooper, A., Burrell-Saward, H., MacLeod, A., and Alsford, S. (2018). Decoding the network of *Trypanosoma brucei* proteins that determines sensitivity to apolipoprotein-L1. PLoS Pathog. *14*, e1006855.
88. Han, J., Pluhackova, K., and Böckmann, R.A. (2017). The multifaceted role of SNARE proteins in membrane fusion. Front. Physiol. *8*, 5.
89. Mion, D., Bunel, L., Heo, P., and Pincet, F. (2022). The beginning and the end of SNARE-induced membrane fusion. FEBS Open Bio *12*, 1958–1979.
90. Itakura, E., Kishi-Itakura, C., and Mizushima, N. (2012). The hairpin-type tail-anchored SNARE syntaxin 17 targets to autophagosomes for fusion with endosomes/lysosomes. Cell *151*, 1256–1269.
91. McLelland, G.L., Lee, S.A., McBride, H.M., and Fon, E.A. (2016). Syntaxin-17 delivers PINK1/parkin-dependent mitochondrial vesicles to the endolysosomal system. J. Cell Biol. *214*, 275–291.
92. Juhász, G. (2016). A mitochondrial-derived vesicle HOPS to endolysosomes using Syntaxin-17. J. Cell Biol. *214*, 241–243.
93. Ebrahim, S., Liu, J., and Weigert, R. (2018). The actomyosin cytoskeleton drives micron-scale membrane remodeling in vivo via the generation of mechanical forces to balance membrane tension gradients. Bioessays *40*, e1800032.
94. Zheng, Q., Bobich, J.A., Vidugiriene, J., McFadden, S.C., Thomas, F., Roder, J., and Jeromin, A. (2005). Neuronal calcium sensor-1 facilitates neuronal exocytosis through phosphatidylinositol 4-kinase. J. Neurochem. *92*, 442–451.
95. Yang, Z., Zhao, X., Xu, J., Shang, W., and Tong, C. (2018). A novel fluorescent reporter detects plastic remodeling of mitochondria-ER contact sites. J. Cell Sci. *131*, jcs208686.
96. Karanasios, E., Walker, S.A., Okkenhaug, H., Manifava, M., Hummel, E., Zimmermann, H., Ahmed, Q., Domart, M.C., Collinson, L., and Ktistakis, N.T. (2016). Autophagy initiation by ULK complex assembly on ER tubulovesicular regions marked by ATG9 vesicles. Nat. Commun. *7*, 12420.
97. Rao, Y., Perna, M.G., Hofmann, B., Beier, V., and Wollert, T. (2016). The Atg1-kinase complex tethers Atg9-vesicles to initiate autophagy. Nat. Commun. *7*, 10338.
98. Matscheko, N., Mayrhofer, P., Rao, Y., Beier, V., and Wollert, T. (2019). Atg11 tethers Atg9 vesicles to initiate selective autophagy. PLoS Biol. *17*, e3000377.
99. Angebault, C., Fauconnier, J., Patergnani, S., Rieusset, J., Danese, A., Affortit, C.A., Jagodzinska, J., Mégy, C., Quiles, M., Cazevieille, C., et al. (2018). ER-mitochondria cross-talk is regulated by the Ca2+ sensor NCS1 and is impaired in Wolfram syndrome. Sci. Signal. *11*, eaaq1380.

100. Garrido-Maraver, J., Loh, S.H.Y., and Martins, L.M. (2020). Forcing contacts between mitochondria and the endoplasmic reticulum extends lifespan in a Drosophila model of Alzheimer's disease. Biol. Open *9*, bio047530.

101. Lim, D., Dematteis, G., Tapella, L., Genazzani, A.A., Calì, T., Brini, M., and Verkhratsky, A. (2021). Ca^{2+} handling at the mitochondria-ER contact sites in neurodegeneration. Cell Calcium *98*, 102453.

102. Rasmussen, M.L., Robertson, G.L., and Gama, V. (2020). Break on through: Golgi-derived vesicles aid in mitochondrial fission. Cell Metab. *31*, 1047–1049.

103. Tábara, L.C., Morris, J.L., and Prudent, J. (2021). The complex dance of organelles during mitochondrial division. Trends Cell Biol. *31*, 241–253.

104. Terriente-Felix, A., Wilson, E.L., and Whitworth, A.J. (2020). *Drosophila* phosphatidylinositol-4 kinase fwd promotes mitochondrial fission and can suppress Pink1/parkin phenotypes. PLoS Genet. *16*, e1008844.

105. Yamashita, S.I., Jin, X., Furukawa, K., Hamasaki, M., Nezu, A., Otera, H., Saigusa, T., Yoshimori, T., Sakai, Y., Mihara, K., and Kanki, T. (2016). Mitochondrial division occurs concurrently with autophagosome formation but independently of Drp1 during mitophagy. J. Cell Biol. *215*, 649–665.

106. Boutry, M., and Kim, P.K. (2021). ORP1L mediated PI(4)P signaling at ER-lysosome-mitochondrion three-way contact contributes to mitochondrial division. Nat. Commun. *12*, 5354.

107. Brown, M.T., Andrade, J., Radhakrishna, H., Donaldson, J.G., Cooper, J.A., and Randazzo, P.A. (1998). ASAP1, a phospholipid-dependent arf GTPase-activating protein that associates with and is phosphorylated by Src. Mol. Cell Biol. *18*, 7038–7051.

108. Liu, X., Shu, S., Billington, N., Williamson, C.D., Yu, S., Brzeska, H., Donaldson, J.G., Sellers, J.R., and Korn, E.D. (2016). Mammalian nonmuscle myosin II binds to anionic phospholipids with concomitant dissociation of the regulatory light chain. J. Biol. Chem. *291*, 24828–24837.

109. Duan, X., Wei, Y., Zhang, M., Zhang, W., Huang, Y., and Zhang, Y.H. (2023). PI4P-containing vesicles from Golgi contribute to mitochondrial division by coordinating with polymerized actin. Int. J. Mol. Sci. *24*, 6593.

110. Dippold, H.C., Ng, M.M., Farber-Katz, S.E., Lee, S.K., Kerr, M.L., Peterman, M.C., Sim, R., Wiharto, P.A., Galbraith, K.A., Madhavarapu, S., et al. (2009). GOLPH3 bridges phosphatidylinositol-4- phosphate and actomyosin to stretch and shape the Golgi to promote budding. Cell *139*, 337–351.

111. Sechi, S., Frappaolo, A., Belloni, G., Colotti, G., and Giansanti, M.G. (2015). The multiple cellular functions of the oncoprotein Golgi phosphoprotein 3. Oncotarget *6*, 3493–3506.

112. Kuna, R.S., and Field, S.J. (2019). GOLPH3: a Golgi phosphatidylinositol(4)phosphate effector that directs vesicle trafficking and drives cancer. J. Lipid Res. *60*, 269–275.

113. Ciarlo, L., Manganelli, V., Garofalo, T., Matarrese, P., Tinari, A., Misasi, R., Malorni, W., and Sorice, M. (2010). Association of fission proteins with mitochondrial raft-like domains. Cell Death Differ. *17*, 1047–1058.

114. Ciarlo, L., Manganelli, V., Matarrese, P., Garofalo, T., Tinari, A., Gambardella, L., Marconi, M., Grasso, M., Misasi, R., Sorice, M., and Malorni, W. (2012). Raft-like microdomains play a key role in mitochondrial impairment in lymphoid cells from patients with Huntington's disease. J. Lipid Res. *53*, 2057–2068.

115. Arasaki, K., Shimizu, H., Mogari, H., Nishida, N., Hirota, N., Furuno, A., Kudo, Y., Baba, M., Baba, N., Cheng, J., et al. (2015). A role for the ancient SNARE syntaxin 17 in regulating mitochondrial division. Dev. Cell *32*, 304–317.

116. Xian, H., Yang, Q., Xiao, L., Shen, H.M., and Liou, Y.C. (2019). STX17 dynamically regulated by Fis1 induces mitophagy via hierarchical macroautophagic mechanism. Nat. Commun. *10*, 2059.

117. Burman, J.L., Pickles, S., Wang, C., Sekine, S., Vargas, J.N.S., Zhang, Z., Youle, A.M., Nezich, C.L., Wu, X., Hammer, J.A., and Youle, R.J. (2017). Mitochondrial fission facilitates the selective mitophagy of protein aggregates. J. Cell Biol. *216*, 3231–3247.

118. Ihenacho, U.K., Meacham, K.A., Harwig, M.C., Widlansky, M.E., and Hill, R.B. (2021). Mitochondrial fission protein 1: emerging roles in organellar form and function in health and disease. Front. Endocrinol. *12*, 660095.

119. Wells, R.C., and Hill, R.B. (2011). The cytosolic domain of Fis1 binds and reversibly clusters lipid vesicles. PLoS One *6*, e21384.

120. Beckerman, P., Bi-Karchin, J., Park, A.S.D., Qiu, C., Dummer, P.D., Soomro, I., Boustany-Kari, C.M., Pullen, S.S., Miner, J.H., Hu, C.-A.A., et al. (2017). Transgenic expression of human APOL1 risk variants in podocytes induces kidney disease in mice. Nat. Med. *23*, 429–438.

121. Muppirala, M., Gupta, V., and Swarup, G. (2011). Syntaxin 17 cycles between the ER and ERGIC and is required to maintain the architecture of ERGIC and Golgi. Biol. Cell *103*, 333–350.

122. Kumar, S., Gu, Y., Abudu, Y.P., Bruun, J.A., Jain, A., Farzam, F., Mudd, M., Anonsen, J.H., Rusten, T.E., Kasof, G., et al. (2019). Phosphorylation of syntaxin 17 by TBK1 controls autophagy initiation. Dev. Cell *49*, 130–144.e6.

123. Hailey, D.W., Rambold, A.S., Satpute-Krishnan, P., Mitra, K., Sougrat, R., Kim, P.K., and Lippincott-Schwartz, J. (2010). Mitochondria supply membranes for autophagosome biogenesis during starvation. Cell *141*, 656–667.

124. Chu, C.T., Ji, J., Dagda, R.K., Jiang, J.F., Tyurina, Y.Y., Kapralov, A.A., Tyurin, V.A., Yanamala, N., Shrivastava, I.H., Mohammadyani, D., et al. (2013). Cardiolipin externalization to the outer mitochondrial membrane acts as an elimination signal for mitophagy in neuronal cells. Nat. Cell Biol. *15*, 1197–1205.

125. Cook, K.L., Soto-Pantoja, D.R., Abu-Asab, M., Clarke, P.A., Roberts, D.D., and Clarke, R. (2014). Mitochondria directly donate their membrane to form autophagosomes during a novel mechanism of parkin-associated mitophagy. Cell Biosci. *4*, 16.

126. Manganelli, V., Capozzi, A., Recalchi, S., Riitano, G., Mattei, V., Longo, A., Misasi, R., Garofalo, T., and Sorice, M. (2021). The role of cardiolipin as a scaffold mitochondrial phospholipid in autophagosome formation: in vitro evidence. Biomolecules *11*, 222.

127. Suen, D.F., Norris, K.L., and Youle, R.J. (2008). Mitochondrial dynamics and apoptosis. Genes Dev. *22*, 1577–1590.

128. Wu, J., Ma, Z., Raman, A., Beckerman, P., Dhillon, P., Mukhi, D., Palmer, M., Chen, H.C., Cohen, C.R., Dunn, T., et al. (2021). APOL1 risk variants in individuals of African genetic ancestry drive endothelial cell defects that exacerbate sepsis. Immunity *54*, 2632–2649.e6.

129. Poudel, B., Vassalotti, A., Wahba, J., Raman, A., Wu, J., and Susztak, K. (2022). Endothelial cell-specific inducible G2 APOL1 risk variant induces hypertension and hypertensive kidney disease in uni-nephrectomy and high-salt mice model. FASEB J *36*, https://doi.org/10.1096/fasebj.2022.36.S1.L7674.

130. Qin, L., and Xi, S. (2022). The role of mitochondrial fission proteins in mitochondrial dynamics in kidney disease. Int. J. Mol. Sci. *23*, 14725.

131. Saleem, M.A., O'Hare, M.J., Reiser, J., Coward, R.J., Inward, C.D., Farren, T., Xing, C.Y., Ni, L., Mathieson, P.W., and Mundel, P. (2002). A conditionally immortalized Human Podocyte Cell Line Demonstrating Nephrin and Podocin expression. J. Am. Soc. Nephrol. *13*, 630–638.

132. Heo, P., Yang, Y., Han, K.Y., Kong, B., Shin, J.H., Jung, Y., Jeong, C., Shin, J., Shin, Y.K., Ha, T., and Kweon, D.-H. (2016). A chemical controller of SNARE-driven membrane fusion that primes vesicles for Ca(2+)-triggered millisecond exocytosis. J. Am. Chem. Soc. *138*, 4512–4521.

133. Heo, P., Coleman, J., Fleury, J.B., Rothman, J.E., and Pincet, F. (2021). Nascent fusion pore opening monitored at single-SNAREpin resolution. Proc. Natl. Acad. Sci. USA *118*, e2024922118.

STAR★METHODS

KEY RESOURCES TABLE

REAGENT or RESOURCE	SOURCE	IDENTIFIER
Antibodies		
Mouse anti-ATG9A	Proteintech	cat# 67096-1; RRID: AB_2882401
Rabbit anti-ATG9A	Abcam	Cat# ab108338; RRID:AB_10863880
Mouse anti-PANX2	Sigma	cat# MABN623
Rabbit anti-MFN2	Abcam	cat# ab124773; RRID: AB_10999860
Mouse anti-FIS1	Santa Cruz Biotechnologies	Cat# sc-376447; RRID:AB_11149382
Rabbit anti-APOL1	Sigma	HPA018885; RRID: AB_1844953
Rabbit anti-PI4KB	Novus Biologicals	NBP1-80907; RRID: AB_11040866
Rabbit anti-PHB2	Proteintech	Cat# 12295-1-AP; RRID:AB_2164779
Goat anti-V5	Novus Biologicals	NB600-380; RRID: AB_10003376
Mouse anti-His tag	Sigma	SAB1305538; RRID: AB_2687993
Mouse anti-S tag	Sigma	SAB2702204
Peroxydase-conjugated goat anti-mouse IgG	Sigma	DC02L; RRID: AB_437851
Chemicals, peptides, and recombinant proteins		
1-hexadecanoyl-2–(9Z-octadecenoyl)-*sn*-glycero-3-phosphocholine	Avanti Polar Lipids	Cat. 850457, PC
1,2-dioleoyl-*sn*-glycero-3-phospho-*l*-serine	Avanti Polar Lipids	Cat. 840035, PS
Cholesterol	Avanti Polar Lipids	Cat. 700000
1,2-dioleoyl-*sn*-glycero-3-phosphoethanolamine	Avanti Polar Lipids	Cat. 850725, PE
L-α-phosphatidylinositol	Avanti Polar Lipids	Cat. 840042, PI
Sphingomyelin	Avanti Polar Lipids	Cat. 860062, SM
Cardiolipin extracts from bovine heart	Avanti Polar Lipids	Cat. 840012, CL
1,2-dioleoyl-*sn*-glycero-3-phosphoethanolamine-N-(7-nitro-2-1,3-benzoxadiazol-4-yl)	Avanti Polar Lipids	Cat. 810145, NBD-PE
1,2-dioleoyl-*sn*-glycero-3-phosphoethanolamine-N-(lissamine rhodamine B sulfonyl)	Avanti Polar Lipids	Cat. 810150, Rhod-PE.
MitoTracker Green FM	Invitrogen	M7514
MitoSOX Red	Invitrogen	M36008
CGSFKEKVSIQNLLLLLTDN EAWNGFVAAAELP	GenicBio	A1HC1
CGSFKEKVSIQNLLLQLTDN EAQNGQVAAQELP	GenicBio	A1HC1mut
CGSVKLTDVAPVSFFLVLDVV YLVYESKHLHEG	GenicBio	A1HC2
CGSVKLTDVAPVSQALVQD VQYLVQESKHLHEG	GenicBio	A1HC2mut
CGSFRERVSPVHLQILLTNN EAWKRFVTAAELP	GenicBio	A3HC1
CGSFRERVSPVHLQIQLTN NEAQKRQVTAQELP	GenicBio	A3HC1mut
CGSARILSATTSGIFLALDV VNLVYESKHLHEG	GenicBio	A3HC2
CGSARILSATTSGQALAQDV QNLVQESKHLHEG	GenicBio	A3HC2mut

(*Continued on next page*)

Continued

REAGENT or RESOURCE	SOURCE	IDENTIFIER
CGSNDRERVNEAREELMRMLAEDELRDA VLLVFANKQDLPNAMNAAEITDKLGLH	GenicBio	ARF1p
CGSDFYLPQLLNMYIHMDEDV GDAIKPYIVHRCRQSINFSLQCALLLGAYS	GenicBio	H1-H3
CGSDFYLPQKLNMKIHMDEDVG DAIKPYIVHRSRQSINFSLQSALLLGAYS	GenicBio	H1-H3mut1
CGSDFYLPQLLNMYIHMDEDVGDA IKPKIKHRSRQSINFSLQSALLLGAYS	GenicBio	H1-H3mut2
CGSDFYLPQLLNMYIHMDEDV GDAIKPYIVHRSRQSINFSLQSALKLGAKS	GenicBio	H1-H3mut3
CGSDFYLPQLLNMYIHMDE DVGDAIKPYIVHRS	GenicBio	H1-H2
CGSIKPYIVHRSRQSIN FSLQSALLLGAYS	GenicBio	H2-H3
CGSMIMKDKNWHDKGQQYRNWFL KEFPRLKSKLEDNIRRLRALADGVQ	GenicBio	L1Hel5
CGSAAIEDEYVQQKDEQFREWF LKEFPQVKRKIQESIEKLRALANGIE	GenicBio	L3Hel5
CGSQAQAHDLVIKSLDKLKE VKEFLGENISNFLSLAGNTYQLT RGIGKDIRALRRAR	GenicBio	L1MAD
CGSEAEASRLTATSIDRLKVFKEV MRDITPNLLSLLNNYYEATQTIG SEIRAIRQAR	GenicBio	L3MAD
KYFKEKVSIQNLLLLLTDNEAWNGFVA AAELPRNEADELRKALDNLARQMIMK	GenicBio	L1NTD
CGSGVKLTDVAPVSFFLVLDVVY LVYESKHLHEGAKSETAEELK KVAQELEEKLNILNNNYKIL	GenicBio	L1CTD
CGSRVSPVHLQILLTNNEAWK RFVTAAELPRDEADALYEAL KKLRTYAAIEDEY	GenicBio	L3NTD
CGSGARILSATTSGIFLALD VVNLVYESKHLHEGAKSASAEE LRRQAQELEENLMELTQI	GenicBio	L3CTD
CGSGRITALNDDINQVVDVM MDNMDKVLARGDRIDTLHERS ATLSEQAQQFQRRSTQLKRNM	GenicBio	TbVAMP7Bp
EEASEGGGNDRVRNLQSE VEGVKNIMTQNVERILARGENLEHLR NKTEDLEATSEHFKTTSQKVARKSGC	GenicBio	VAMP8p
Recombinant PI4KB	ThermoFisher	PR9008A
Recombinant NCS1	Antibodies-online	ABIN2130777
Recombinant NCS1	Uzureau et al.[11]	N/A
Reccombinant NCS1 L89K	Uzureau et al.[11]	N/A
Recombinant Calneuron-1	Novus Biologicals	NBP1-50858
Recombinant Calneuron-1	Prospec	pro-279
Recombinant PHB2	Origene	TP760501
Recombinant VAMP8	Abnova	8673-P01
Recombinant VAMP8	Novus Biologicals	NBC1-18348
Recombinant VAMP8	Heo et al.[132]	N/A
Recombinant sVAMP8	Heo et al.[132]	N/A
Recombinant SNAP25	Heo et al.[132]	N/A

(*Continued on next page*)

Continued

REAGENT or RESOURCE	SOURCE	IDENTIFIER
Recombinant STX1A	Heo et al.[132]	N/A
Recombinant APOL1	This study	N/A
Recombinant APOL1Δ	This study	N/A
Recombinant APOL3	This study	N/A
Recombinant APOL3Δ	This study	N/A
Recombinant ARF1	This study	N/A
Critical commercial assays		
ADP-Glo kinase assay kit	Promega	V6930
Phosphoinositides, Strip	Echelon Biosciences	P-6001-2
Ni-NTA beads	QIAGEN	30210
Experimental models: Cell lines		
Human: immortalized podocyte cell line (WT, wild-type)	Saleem et al.[131]	N/A
APOL1-KO human podocyte cell line	Uzureau et al.[11]	N/A
APOL3-KO human podocyte cell line	Uzureau et al.[11]	N/A
APOL1Δ human podocyte cell line	Uzureau et al.[11]	N/A
Recombinant DNA		
Phb2 (NM_007531) Mouse Tagged ORF Clone	OriGene	Cat#: MR218376
pEX-A128-ARF1D13	Eurofins Genomics	aP37C-3
Software and algorithms		
ImageJ	NIH	https://hpc.nih.gov/apps/Fiji.html
Graph-pad Prism 10	Graphpad prism	https://www.graphpad.com
Amira	Thermo Fisher Sci.	https://www.thermofisher.com>amira
Ilastik	Ilastik	https://www.ilastik.org/
Other		
Biosensor/Streptavidin (SA) Pack	ForteBio/Molecular Devices	Ca#18-5020

RESOURCE AVAILABILITY

Lead contact and materials availability

Further information and requests for reagents may be directed to, and will be fulfilled by the corresponding author Etienne Pays (etienne.pays@gmail.com).

Materials availability

All unique/stable reagents generated in this study are available from the Lead Contact with a completed Materials Transfer Agreement.

Data and code availability

- The data reported in this paper are available upon request from the lead contact.
- This paper does not report original code.
- Any additional information required to reanalyze the data reported in this work paper is available from the lead contact upon request.

EXPERIMENTAL MODEL AND STUDY PARTICIPANT DETAILS

In vitro culture of human podocytes

The APOL1-KO, APOL3-KO and APOL1Δ podocyte cell lines were derived from immortalized wild-type human podocytes[131] through CRISPR-Cas9-mediated editing of the APOL1 or APOL3 genes, as described in Uzureau et al.[11] and repeated below. Cells were grown to confluence at 33°C, at which point they were trypsinized and reseeded in fresh flasks at a dilution of between 1:3 and

1:5. Before thermoswitching to 37°C, cells were grown to 70 to 80% confluence. At both temperatures, cells were fed with fresh medium 3 times per week. Podocytes were used after 7 to 14 days of differentiation.

METHOD DETAILS

The methods used to generate, cultivate and characterize the podocyte cell lines were described in every detail in Uzureau et al.[11] This involves CRISPR-Cas9-mediated editing of the APOL1 or APOL3 genes, as well as the characterization of the cellular phenotypes, the representativity of the phenotype of the selected cell lines and the entire genome sequencing of these cell lines, as well as the validation of the antibodies used for APOLs detection. In case of APOL3, a sequence encoding the V5 epitope was grafted by CRISPR-Cas9-mediated gene targeting to the 3′end of the APOL3 open reading frame to enable detection of APOL3 with V5 antibodies.

Generation of *APOL*-edited podocytes

CRISPR-Cas9 and green fluorescent protein (GFP) fusion protein expression vectors U6gRNA-Cas9-2A-GFP guide were purchased from Sigma-Aldrich.[11] These vectors allow the co-expression of GFP and Cas9 from the same mRNA via a 2A peptide linkage, which enables tracking of transfection efficiency. Plasmids were transfected into podocytes using Cell Line Nucleofector Kit V (Lonza, Bale, Switzerland) and program T-020 (2 μg plasmid per 2 x 10^6 podocytes) with Nucleofector II apparatus (Lonza) following manufacturer's instructions. The GFP positive cells were sorted using a FACSAria III cell sorter (BD Biosciences, Franklin Lakes, USA) and seeded at one cell per 3 wells in 96 well-plates. The clones were screened by Western blot analysis for the lack of targeted APOL expression. The genomic DNA of the selected clones was extracted using the Quick-DNA Plus kit (Zymo Research, Irvine, USA) following manufacturer's instructions. The genomic region targeted by the CRISPR/Cas9 procedure was amplified by PCR and cloned into pGEM-Teasy vector (Promega). Ten clones were sequenced and the genome of podocyte cell lines chosen to pursue the study was fully sequenced.

In situ C-terminal tagged versions of APOL3

All the anti-APOL3 antibodies that were tested, either raised in our laboratory or commercially available, exhibited non-specific reaction. Therefore, we generated podocyte cell lines which express the V5, TriFlag or GFP tags in fusion with APOL3. The CRISPR-Cas9 and E2 Crimson fluorescent protein expression vector pSpCas9(BB)-2A-E2Crimson was generated as follow. The T2A fragment was PCR-amplified from pSpCas9(BB)-2A-GFP vector using the 5′- CCGGCCAGGCAAAAAAGAAAAAGG -3' and 5′- AGTGCTATCCACTGGGCCAGGATTCTCCTCG – 3' primers. The E2-Crimson fragment was PCR-amplified using the 5′- TGG CCCAGTGGATAGCACTGAGAACGTCAT -3' and 5′- GCTGATCAGCGAGCTCTAGTTAGCCCTGGAACAGGTGGTGGCGGG -3' primers. The T2A and E2-Crimson fragments were cloned into EcoRI digested pSpCas9(BB)-2A-GFP vector using NEBuilder HiFi DNA Assembly Master Mix (New England Biolabs, Ipswich, USA) following manufacturer's instructions to generate pSpCas9(BB)-2A-E2Crimson. The CRISPR-Cas9 guide RNA sequence targeting *APOL3* was generated by cloning the annealed 5′- CACCG CACTGGTCTGGGGTCAGT -3' and 5′- AAACACTGACCCCAGACCAGTGC -3' primers into the BbsI restricted pSpCas9(BB)-2A-E2Crimson vector.

The C-terminal APOL3 tagging constructs pApoL3-HRV-V5-2A-GFP and pApoL3-HRV-TriFlag-2A-GFP were generated as follow. The *APOL3* ORF and *APOL3* UTR fragments were PCR-amplified from podocyte gDNA using respectively the 5′- TTGCATGCCTGCA GGTCGACTATGAGGCAGATGCTCTCTACG -3' and 5′- ACTTCCCAGCGGGCCCTGGAACAATACTTCCAGATCACTGCCGTGGGT ATGGCATGGATTCAGA -3' primers, and the 5′- CTGTACAAGTAGCCCCAGACCAGTGCAGCC -3' and 5′- AATTCGAGCTCGG TACCCGGGTTACACACAGGGCACTCAGC -3' primers. The V5-GFP and TriFlag-GFP fragments were PCR-amplified from the pSpCas9(BB)-2A-GFP vector S1 using respectively the 5′- CCAGGGCCCGCTGGGAAGTGGCAAACCGATTCCGAACCCGCTT CTTGGTCTAGACAGCACCGGTGGCAGTGGAGAGGGCAGA -3' and 5′- GTCTGGGGCTACTTGTACAGCTCGTCCATGCC -3' primers, and the 5′- CCAGGGCCCGCTGGGAAGTGATTATAAGGATCATGATGGTGACTACAAAGACCATGATATCGATTACAAAGA TGATGACAAGGGTGGCAGTGGAGAGGGCAGA -3' and 5′- GTCTGGGGCTACTTGTACAGCTCGTCCATGCC -3' primers. The *APOL3* ORF, *APOL3* UTR and either V5-GFP or TriFlag-GFP fragments were cloned into XbaI/BamHI restricted pUC18 vector using NEBuilder HiFi DNA Assembly Master Mix (New England Biolabs) following manufacturer's instructions to generate the pAPOL3-HRV-V5-2A-GFP or pAPOL3-HRV-TriFlag-2A-GFP tagging constructs respectively. The tagging constructs were linearized using SalI and KpnI restriction enzymes before use.

Podocytes were transfected using *APOL3*-targeted pSpCas9(BB)-2A-E2Crimson vector and pAPOL3-HRV-V5-2A-GFP vectors to generate the WT TriFlag, WT 3V5, 1 Δhom 3V5 and 1KO 3V5 cell lines. Both induction of cell death and APOL3 expression by poly(I:C) remained unaltered in the podocyte cell lines expressing V5-tagged APOL3.

SPR analysis

All peptides (>90% pure) were obtained from GenicBio (Shanghaï, China). Peptide-peptide interactions were studied by SPR on a Biacore 3000 (GE Lifesciences, Brøndby Denmark). Peptides were immobilized on a CM5 sensor chip (GE Lifesciences) using the Thiol Coupling Kit (GE Lifesciences) essentially according to the manufacturer's instructions. Briefly, peptides containing an N-terminal cysteine residue were diluted to 50 μg/mL in 10 mM Na phosphate buffer (pH 4.0) and immobilized at surface densities ranging

from 0.3 to 1.2 pmol/mm. Flow cells were regenerated with two injections of 10 μL 100 mM glycine, 5 mM EDTA, 500 mM NaCl, 0.05% Tween 20 (pH 3.0) at 10 μL/min. Binding parameters were determined by fitting to a 1:1 interaction model using the BIAevaluation 4.1.1. (GE Lifesciences). Each parameter was determined by a duplicate run of duplicate factor 2 dilution series of dissolved peptide, ranging from 1.25 to 20 μM. As a minimum all experiments were conducted in triplicates of duplicates.

BLI analysis

Biotinylated PI4KB, NCS1 or CALN1 (10 μg/mL) were captured by pre-hydrated streptavidin biosensors (Pall ForteBio) in BLI running buffer (10 mM HEPES, 150 mM NaCl, 0.05% Tween 20, 0.1% BSA, pH 7.4 or pH 6.4) containing 50 μM $CaCl_2$ or 10 mM EGTA. Association and dissociation of equimolar amounts of APOL variants were measured for 600–1000 s. All sensorgrams were aligned to the baseline and a Savitzky-Golay filter was applied to smooth the data.

PI4KB activity measurements

Recombinant PI4KB, APOL1, APOL3, NCS1 and CALN1 were diluted in 96 well-plates in kinase buffer (50mM NaCl, 2 mM $MgCl_2$, 25 mg/mL BSA, 0.04% Triton X-100, 50 mM DTT, 4 mM $MnCl_2$, 100 mM HEPES pH 7.5) containing either 0.5 mM EGTA, 0.1 mM $CaCl_2$ or 2 mM $CaCl_2$. After preincubation for 10 min at room temperature, the PI4KB substrate (PI:PS mix) was added. Reaction was started by addition of 40 mM ATP and incubated for 40 min at 30°C. ADP was revealed by ADP-Glo kinase assay kit (Promega) following manufacturer's instruction. Background activity was evaluated by omission of either IP substrate, ATP or PI4KB, and was always lower than 0.1%.

In vitro lipid binding assays

Lipid binding assays were performed on lipid-coated strips. Briefly, nitrocellulose membranes prespotted with various indicated lipid species (P-6001, P-6002, Echelon, Salt Lake City, UT) were blocked in 3% fat-free BSA for 60 min at room temperature, probed with recombinant sVAMP8 (100 ng/mL) in 3% fat-free BSA in TBST for 1 h at room temperature, followed by anti-His mouse monoclonal antibody and peroxydase conjugated anti-mouse antibody, and ECL detection and imaging.

Immunoprecipitation

Protein lysates in RIPA buffer with 1% NP-40 or 1% CHAPS (300 μg–1 mg) were incubated with primary antibody overnight at 4°C, followed by incubation with 20 μL of pre-blocked protein G-Sepharose beads for 1 h. Following four washes in RIPA buffer and one wash in PBS, the immune complexes were eluted in non-reducing Laemmli buffer and analyzed by Western blotting.

Immunofluorescence

Cells were grown in Falcon culture chambers (8 wells plate). PBS-washed cells were fixed in 4% paraformaldehyde for 10 min at room temperature, treated with 0.1% (v/v) Triton X-100 in Tris-buffered saline for 10 min and incubated for 1 h in Tris-buffered saline with 5% bovine serum albumin. Nuclei were stained with DAPI. Co-localization analysis was performed using JACoP (Just Another Colocalization Plugin) for ImageJ. The co-localization was quantified using Manders coefficients calculated after Costes automated threshold.

pDUET assays

Cultures of BL21(DE3) strains transfected with pCDF-Duet1 constructs were grown at 37°C in LB containing 50 μg/mL streptomycin and 1% glucose from freshly plated colonies until OD600 reached 0.7 to 0.8. Cultures were centrifuged and bacteria pellet was resuspended in fresh medium without glucose and distributed in 3 flasks to perform induction and copurification in triplicate. Expression of recombinant proteins was induced by addition of 1mM IPTG overnight at 20°C and 80 rpm. Cell density was measured by OD600 and bacteria were centrifuged and resuspended in (10% of culture volume × OD600) in cold hypotonic buffer (50 mM MES pH 6.0 or pH 7.0) containing EDTA-free protease inhibitors (Roche). Bacteria were lysed by Fast Prep 24 (MP Biomedicals) with 1/10 volume of glass beads (Lysing Matrix B, MP Biomedicals), for 3 × 30 s at 6 m/s. Cell lysate was complemented by 0.6 M NaCl, 1% Triton X-100, 20 mM imidazole, and vortexed vigorously. Cell debris were pelleted by centrifugation for 15 min at 16,000 g, and the supernatant was applied onto Ni-NTA beads (Qiagen) equilibrated in the same buffer, for 2 h at 4°C. After binding the beads were washed with 20 volumes of beads with cold binding buffer and the bound proteins were eluted with 2 volumes of SDS-PAGE sample buffer. Supernatant (total soluble fractions) and bound fractions were analyzed by western blotting. His tag was revealed with anti-His mouse monoclonal antibody and peroxydase conjugated anti-mouse antibody. Stag was detected by anti-Stag monoclonal antibody (Novagen) and peroxydase conjugated anti-mouse antibody. Peroxydase activity was revealed by ECL (Western Lighting Chemiluminescence Reagent PLUS, PerkinElmer).

Membrane fusion assays

Full-length VAMP8, SNAP25, STX1A and cytosolic VAMP8 (sVAMP8) were purified as described in Heo et al.[132] The following lipids were used for vesicle formation: 1-hexadecanoyl-2–(9Z-octadecenoyl)-*sn*-glycero-3-phosphocholine (PC), 1,2-dioleoyl-*sn*-glycero-3-phospho-*l*-serine (PS), Cholesterol (Chol), 1,2-dioleoyl-*sn*-glycero-3-phosphoethanolamine (PE), L-α-phosphatidylinositol (PI), Sphingomyelin (SM), Cardiolipin extracts from bovine heart (CL), 1,2-dioleoyl-*sn*-glycero-3-phosphoethanolamine-N-(7-nitro-2-1,3-benzoxadiazol-4-yl) (NBD-PE) and 1,2-dioleoyl-*sn*-glycero-3-phosphoethanolamine-N-(lissamine rhodamine B sulfonyl)

(Rhod-PE). Each protein was reconstituted into small unilamellar vesicles (SUVs) following a co-micellization protocol.[133] In brief, VAMP8 (800:1 lipid to protein ratio) and HK buffer (25 mM HEPES, 150 mM KCl, pH 7.4) containing 1% octyl-β-*d*-glucopyranoside (OG) were used to resuspend the lipid film containing PC:PS:Chol:PE:SM:PI:N-PE:R-PE (27:2:30:17:15:6:1.5:1.5 mol%, total 3 mM lipids). Each APOL and HK buffer with 1% OG were used to resuspend the film containing PC:PS:PE:PI:CL (33:2:30:13:22) or PC:PS:PE:PI (55:2:30:13:22, no CL) at a 1000:1 lipid to protein ratio. For SNAP25/STX1A (denoted Q-SNARE), the same lipid composition as in the APOL cases was used at a 400:1 lipid to protein ratio. These protein(s)/lipids mixtures were vortexed at room temperature for 2 h, diluted with HK buffer two times, and dialyzed at 4°C overnight. Each pair of VAMP8-SUVs and APOL- or STX1A/SNAP25- SUVs was mixed in 9:1 mol% (total 1 mM lipids) in 96-well plates. Either 10 μM sVAMP8 or protein-free SUVs (N/R-SUV) was used as negative control. The dequenching signal of NBD-PE was measured at 37°C for 90 min and for 5 min after addition of 1% Triton.

FIB-SEM imaging

Samples were incubated in fixative (2% paraformaldehyde (PFA, Applichem), 2.5% glutaraldehyde (GA, EMS) in 0.15M Sodium Cacodylate (Sigma-Aldrich) buffer, pH 7.4) at room temperature (RT) for 30 min. Fixative was removed by washing 5 × 3 min in 0.15M cacodylate buffer and samples were incubated in 1% osmium (OsO_4, EMS), 1.5% potassium ferrocyanide (Sigma-Aldrich) in 0.15M cacodylate buffer for 40 min at RT. This was immediately followed by a second incubation in OsO4 (1% Osmium in double distilled H_2O (ddH_2O) for 40 min at RT. After washing in ddH_2O for 5 × 3 min, samples were incubated overnight at 4°C in 1% Uranyl Acetate (UA, EMS). Uranyl acetate was removed by washing in ddH_2O for 5 × 3 min and subsequently dehydrated and embedded as indicated above. Embedded samples were then mounted on aluminum SEM stubs (diameter 12 mm) and coated with ∼8nm of Platinum (Quorum Q150T ES). FIB-SEM imaging was performed using a Zeiss Auriga Crossbeam system with Atlas3D software. The Focused Ion Beam (FIB) was set to remove 5 nm-sections by propelling Gallium ions at the surface. Imaging was done at 1.5 kV using an ESB (back-scattered electron) detector. 3D reconstruction and segmentation were generated from the image stacks using Fiji ImageJ (NIH, USA) ilastik and Amira (Thermo Fisher Sci.) softwares.

QUANTIFICATION AND STATISTICAL ANALYSIS

Statistical analysis was performed using Prism software (GraphPad). Immunofluorescence data were obtained from randomly selected cells from three independent experiments, and the images shown are representative of the majority of cells. Quantitative data were represented as means ± standard deviation (SD); n = 3 unless otherwise indicated in the figure legends; no sample was excluded. p values were calculated by the Mann-Whitney test (*$p < 0.05$; **$p < 0.01$; ***$p < 0.001$; ****$p < 0.0001$).